Article:

Wood, AM, Paton, DA, Collier, REL et al. (1 more author) (2015) Understanding regional scale structural uncertainty: The onshore Gulf of Corinth Rift as a hydrocarbon exploration analogue. Interpretation, 3 (4). SAC35 - SAC53. ISSN 2324-8858

https://doi.org/10.1190/INT-2015-0046.1

Interpretation™

Understanding Regional Scale Structural Uncertainty: The Onshore Gulf of Corinth Rift as a Hydrocarbon Exploration Analogue

Journal:	*Interpretation*
Manuscript ID:	INT-2015-0046.R1
Manuscript Type:	Geophysical modeling for interpreters
Date Submitted by the Author:	18-Jul-2015
Complete List of Authors:	Wood, Alan; Shell Global Solutions Netherlands, Paton, Douglas; University of Leeds, Basin Structure Group Collier, Richard; University of Leeds, Basin Structure Group O'Connor, Viki; Scarabus Geological Consulting Ltd,
Keywords:	modeling, geology, faults, 2D, ray tracing
Subject Areas:	Structural, stratigraphic, and sedimentologic interpretation, Outcrop and subsurface modeling, Volumetrics, uncertainty, and risk analysis, Interpretation concepts, algorithms, methods, and tools, Tutorials/pitfalls and lessons learned

Understanding Regional Scale Structural Uncertainty: The Onshore Gulf of Corinth Rift as a Hydrocarbon Exploration Analogue

ABSTRACT

A major challenge when exploring for hydrocarbons in frontier areas is a lack of data coverage. Data may be restricted to regional scale 2D seismic lines, from which assumptions of the 3D geometric configuration are drawn. Understanding the limitations and uncertainties when extrapolating 2D data into 3D space is crucial when assessing the requirements for acquiring additional data such as 3D seismic or exploration wells, and of assigning geologically reasonable uncertainty ranges.

The Onshore Gulf of Corinth Rift provides an excellent analogue for rift-scale structural uncertainty in the context of hydrocarbon exploration. Here we use seismic forward modelling to explore this area of uncertainty. Synthetic seismic sections have been generated across the rift based upon fault geometries mapped in the field. Comparison of these sections with the mapped geometries allows quantification of uncertainties encountered when extrapolating 2D data into three dimensions. We demonstrate through examples how potential column heights may be both severely over- and under-estimation due to trap integrity, spill point depth and fault seal ambiguities directly related to fault geometric uncertainty. In addition, fault geometries and linkages also control the location of hanging wall syn-rift reservoirs. Hence, gross reservoir volumes and sediment facies distributions are also significantly influenced by how fault geometries are extrapolated along-strike from 2D to 3D.

INTRODUCTION

In a hydrocarbon exploration setting relay zones often define structural spill points, and can hence control the potential volume of hydrocarbon within a trap. Typically only sparse 2D seismic data is available during the exploration phase, leading to significant uncertainty in along-strike displacement variations and the locations of relay zones. This is in addition to other uncertainties inherent in seismic acquisition, such as migration and velocity uncertainties. Fault geometric uncertainty therefore potentially has significant implications for the volumetrics, and ultimately the economic viability, of a prospect.

The aim of this study is to use the fault and syn-rift stratigraphic geometries identified from integration of both new (Wood, 2013) and previously published (Collier and Gawthorpe, 1991, 1995; McNeill et al., 2005, 2007; Bell et al., 2009, 2011) field data from the onshore Gulf of Corinth rift (Figure 1) as a case study to explore some of the fault related geometric uncertainties which may be encountered during hydrocarbon exploration where only limited data may be available. A number of the potential implications for volumetrics and producibility of this geometric uncertainty are also examined. A series of 2D synthetic seismic sections have been generated across a 3D geological model constructed from field data. Comparison of the relatively well constrained mapped geometries with those geometries identifiable from the synthetic seismic sections allows the influence of uncertainty in along-strike displacement continuity to be explored.

Fault Geometric Uncertainty During Hydrocarbon Exploration

Faults influence hydrocarbon exploration in a number of ways, including through the formation of traps, influencing trap and seal integrity, and controlling subsidence and hence maturation history. In addition, faulting also controls and modifies syn-rift sediment distribution and stratigraphic architecture. During the exploration phase of hydrocarbon development, data are typically sparse, hence the magnitude of the influence of faults is often uncertain. Here, the Gulf of Corinth rift is used as an analogue for investigating reservoir volumetric uncertainties, firstly through trap geometry in the form of tilted footwall fault blocks and secondly through the distribution of syn-rift reservoir facies within hanging wall basins. In both instances, the extrapolation of 2D data into the third dimension is critical when estimating potential volumes and evaluating cross fault connectivity and likely producibility.

Tilted Fault Blocks and Volumetrics

A common trap geometry in extensional provinces is that of the tilted fault block (Struijk and Green, 1991; Yielding and Roberts, 1992; Dominguez, 2007). During extensional faulting a combination of elastic (McKenzie, 1978; Barr, 1987; Jackson and McKenzie, 1988) and flexural (Kuznir et al., 1991, 1995) processes lead to reverse drag adjacent to normal faults. This drag takes the form of basin-forming subsidence in the hanging wall and uplift of the footwall (Yielding and Roberts, 1992). The wavelength of the reverse drag is proportional to the elastic thickness of the crust with the relative amplitudes of footwall uplift and hanging wall subsidence controlled by loading of the hanging wall (Jackson and McKenzie, 1983). A low density load, such as water, will allow greater footwall uplift, whilst a denser load, such as a syn-rift stratigraphy, will increase subsidence of the entire local lithosphere, including both the hanging wall and footwall. The relief generated by footwall uplift provides a trapping structure for buoyant hydrocarbons. Aside from the petrophysical properties of the reservoir (porosity, fluid saturation etc.), the volume of hydrocarbon which can be trapped depends on the interplay between along-strike displacement continuity and the thickness of the reservoir interval. This is often visualised using Allan diagrams and juxtaposition/triangle diagrams (Allan, 1989; Knipe, 1997). Where displacement is less than reservoir thickness, fluid can potentially flow across the fault into the adjacent fault block. Hydrocarbon column heights which can be supported by the fault are therefore dependent on both the fault geometry and the fault rock petrophysical properties (Yielding et al., 1997, 2010; Fisher and Knipe, 1998; Sperrevik et al., 2002). Conversely, where displacement is greater than reservoir thickness a juxtaposition seal can be formed between the adjacent fault blocks where units of contrasting permeability are juxtaposed and no shallower hanging wall units are in proximity. In this instance, the hydrocarbon column height is controlled by the structural spill point. The location of the structural spill point will generally be at displacement minima, such as relay zones, however the likelihood that a 2D seismic section will intersect a displacement minima is low. Therefore, being able to predict and account for along-strike displacement minima is critical in order to prevent trap volumetrics from being overestimated.

Syn-Rift Reservoir Facies Distribution

Faults can also control the distribution of reservoir facies within their hanging walls, both through sediment dispersal and basin entry points (Gupta et al., 1999) and the general sub-basin geometry (Dawers and Underhill, 2000; Cowie et al., 2000; McLeod et al., 2002), as well as influencing reservoir quality and facies (Brehm, 2003; Fletcher, 2003). Where only 2D seismic data is available, correlating the extent of syn-rift deposits between sparse sections is highly uncertain and can depend upon the evolution, linkage and growth of the fault system (Mortimer et al., 2007).

Top Seal Integrity

In addition to unconstrained volumetric estimates, the uncertainty in hydrocarbon column heights leads to inexact predictions of pressure due to buoyancy within reservoir intervals. Estimating the maximum column height within a fault-controlled trap depends on correctly identifying the crest of the trapping structure, as well as its spill points. If the geometry allows for a greater column height than is predicted from 2D seismic data, then the buoyancy pressure at the crest of the structure will be greater than anticipated. This may have major implications for trap integrity. A top seal can be breached in two main ways, firstly due to membrane leakage where the buoyancy pressure at the crest of the trap exceeds the capillary entry pressure of the top seal (Schwolater, 1979; Watts, 1987; Ingram and Urai., 1999). Where a top seal has a very high capillary entry pressure, such as for low permeability shales, the second mechanism of breaching through the formation of hydraulic fractures may occur (Swarbrick et al., 2010; Zhang and Ghassemi., 2011). Hence, understanding potential uncertainty in trap crest and spill point location is important when extrapolating 2D into 3D.

METHODOLOGY

The fault geometries and syn-rift stratigraphic architecture from the onshore Gulf of Corinth rift are well studied, with numerous publications focussing on mapping both the onshore outcrop pattern and offshore fault network (e.g. Collier and Gawthorpe, 1991, 1995; McNeill et al., 2005, 2007; Bell et al., 2009, 2011). Here we focus on the onshore portion of the rift, since the addition of further mapping (Wood, 2013) better constrains the syn-rift outcrop pattern and fault network geometry when compared to the 2D seismic data used to map the offshore area. The anticedant drainage pattern cross-cutting the fault blocks provides numerous sub-parallel dip sections allowing well constrained fault geometries, sediment thicknesses and throw distributions to be mapped out. In addition, the recent timing of the rift (Pliocene to recent, Ford et al., 2012) means that erosion has been relatively limited. As a result, the crests of footwall blocks are largely intact, with their elevations being excellent proxies for the along strike variation in displacement. The combination of mapped fault traces, facies distributions and dip sections allows the 3D geometry of the area to be relatively well constrained. Nethertheless, areas of non-exposure still lead to some degree of uncertainty, notably in the west of the field area (figure 1).

Extrapolation of fault geometries into the subsurface using orientation data collected from exposed fault planes allows an approximation of the 3D fault network geometry to be captured and modelled within a geocellular grid (figure 2). The generation of synthetic seismic sections, at a spacing of 5 km, across this grid allows the geometries to be observed in the context of a hydrocarbon exploration scenario, where the limitations of sparse 2D data lead to significant geometric uncertainty.

The procedure for generating the synthetic seismic sections is a four-step process, similar to that used by Wood et al, (2015). Initially the geocellular grid capturing the 3D fault geometries is translated from its physical elevation into the subsurface. The geometry of the mapped pre-rift and syn-rift zones are modelled, as well as an overlying zone of post-rift shale designed to represent a regional top seal. These zones are stochastically populated with mineralogical fractions using a sequential Gaussian distribution function. Upper and lower bounds for the pre- and syn-rift sequences broadly correspond to those observed in the field area, whilst the post-rift composition is a synthetic, shale dominated composition (table 1). Since the rift is still active, there is no post-rift sequence to use as an analogue. A porosity property based on published generalised depth trends for carbonate, conglomerate and shale, is also defined (figure 3), with the upper and lower bounds based upon observation of thin sections from the field area. Examples of the populated grids are shown in figure 4.

An oil-water contact is assigned at a constant depth of 3500 m, with hydrocarbon saturations of 0.7 within the oil leg and zero elsewhere. These values represent those typically expected in a water-wet reservoir (Ahmed, 2010). Pore pressures are assigned separately for the pre-, syn-, and post-rift stratigraphies within the model (figure 5). The post-rift is assigned a hydrostatic gradient of 9.792 MPa/km (0.433 psi/ft), with the underlying pre- and syn-rift strata modelled as being overpressured by 5 MPa (725 psi). The oil column within the syn-rift has a pressure gradient of 6.785 MPa/m (0.3 psi/ft). The petrophysical, mineralogical and pressure properties are converted into individual high resolution seg-y volumes covering the positions where seven synthetic seismic sections will be generated (figures 6, 7). These seg-y property cubes are subsequently exported to seismic forward modelling software.

To account for seismic wave propagation, attenuation and diffraction along the travel path between the seismic sources and the receivers, a coarse scale grid (250 x 250 x 33 m cell dimensions) capturing the properties of the overburden was constructed (figure 8). The overburden is representative of a regional shale, and is hence populated using the same methodology (sequential Gaussian simulation) and property bounds used to generate the synthetic post-rift interval. These properties are also exported to the seismic forward modelling software to be used in conjunction with a ray-tracing algorithm (Gjøystdal et al., 2007).

The seg-y property cubes are imported into the seismic forward modelling software, where density values for the individual mineralogical and fluid components are assigned (Table 2) and used to calculate the overall density assuming a Reuss mixing model (Reuss, 1929). The pore fluid pressure property is used to estimate the confining pressure and the effective pressure based upon a lithostatic gradient of 22.5 MPa/km. Gassmann's theory is then applied along with the fluid properties (Table 2) and saturation distribution to determine the elastic properties of the model, with reflectivity subsequently calculated using the Zoeppritz equations (Zoeppritz, 1919; Gjøystdal et al., 2007).

A 2D seismic survey with a design typical for exploration purposes (O'Dowd, pers. comm.) was constructed (Table 3), with this geometry repeated to correspond to the position of each target section (figure 9).

The derived elastic and reflectivity properties are combined with the survey design, input wavelet, and background model (figure 8), to generate a series of synthetic 2D seismic sections (figure 10) using a ray-tracing algorithm (Gjøystdal et al., 2007). These sections are then interpreted using standard seismic interpretation software, with faults, top pre-rift and top syn-rift surfaces being interpreted. The interpretation was carried out independently by a third party so as to minimise interpretation bias. The seismic interpretations for the seven 2D sections (figure 11) were extrapolated using a convergent interpolation algorithm in order to generate 3D surfaces for the faults, and the top pre-rift and syn-rift stratigraphic surfaces (figure 12). These surfaces allow the construction of a fault-horizon model analogous to those used during hydrocarbon exploration and prospect identification, risking and ranking. Comparison of the models constrained using 3D outcrop data and the model derived from synthetic seismic data, allows exploration scale geometric uncertainty to be quantified in a number of ways, for example by comparing fault-displacement profiles (figure 13). Displacement profiles represent total basement offset and are comparable to those observed by others (Roberts and Koukouvelas, 1996; McNeill et al., 2007; Bell et al., 2011). For the outcrop geometries, where direct measurements are not available, the displacement is calculated by projecting the hanging wall dip slope towards its intersection with the fault plane. For the synthetic seismic derived model the values are derived directly from the model.

RESULTS

Syn-Rift Reservoir

To a large extent, fault geometries control the distribution, thickness and volume of syn-rift sediments within hanging wall basins. In the Gulf of Corinth rift, from which the synthetic seismic sections are generated, the volumetric majority of continental syn-rift deposits do not form a viable reservoir due to the high proportion of low net:gross overbank shale facies. Despite the basin-fill not being of a reservoir facies, geometrically the basins are very similar to many exploration provinces. In such situations mapping the extent of the syn-rift facies would be crucial when generating volumetric estimates. Where only 2D seismic data exists, the 3D extent of a facies is significantly uncertain, with limited constraint on the location of fault displacement minima which often control facies distribution (Athmer and Luthi, 2011). Field data offers a significant improvement over 2D data in this respect, although it is still limited by the level of outcrop exposure and difficulty of extrapolating geometries into the subsurface.

Connected Volume

Connectivity of reservoir facies in the hanging wall block of a fault set depends upon a balance between the evolutionary maturity of the fault set and the sediment input rate into the depocentre (Gawthorpe et al., 1994). This balance is known as the accommodation to supply ratio (A:S), and controls whether a basin is underfilled or overfilled (Jervey, 1988). Accommodation is controlled by subsidence on faults and sea level variations, whilst sediment supply is predominantly a function of climate and hinterland uplift. Fault growth processes (i.e. linkage of fault segments) lead to along-strike variations in displacement and displacement rates, and hence on generation of accommodation space, in turn influencing connectivity of hanging wall sediments. We can observe this influence in the sediment thickness isochore data for the models (figure 14). Although the isochore data are generally of a coarse resolution, it does highlight broad scale changes in sediment package thickness. Where linkage of fault segments has occurred relatively early during fault set growth, profile readjustment (Cowie et al., 2000; Paton, 2006) may lead to sediment thicknesses which vary consistently along-strike (e.g. Tsivlos fault, see figure 1). Where segments have not linked, or have linked late, topographic highs ('Intra Basinal Highs', Cowie et al., 2000) at relay zones may act as barriers to the amalgamation of sub-basin sediments (e.g. Dhemesticha-Kalavryta fault set, figures 1, 14). In turn this affects the connectivity of the syn-rift reservoir facies (figure 15), with implications for connected volume and hence producbility.

For the outcrop-based model, where syn-rift sediment distribution has been mapped in the field (Collier and Gawthorpe, 1991, 1995; McNeill et al., 2005, 2007; Bell et al., 2009, 2011; Wood, 2013), connectivity is high between sub-basins, with a connected pore volume of 1.1×10^{11} m^3 (assuming 10% porosity). In an exploration scenario where the syn-rift represents the target reservoir facies this would be advantageous. Interpretation of the sparse 2D synthetic seismic sections (which are generated using the outcrop-based geometry) leads to significant uncertainty in the distribution of the syn-rift facies, in this case leading to lower connectivity between sub-basins. Based on this interpretation three distinctly separate prospects exist with pore volumes of 4.7×10^9 m^3, 4.6×10^{10} m^3 and 5.4×10^{10} m^3.

Spill Point and Column Height

Uncertainty in syn-rift distribution, where only sparse data is available, also effects estimates of the depth of structural spill points, and hence of potential hydrocarbon column heights. The spacing of 2D data (in this case 5 km) means that it is unlikely that the structural spill point will be intersected and directly identified, but that it will be based upon lateral projection of the available data. Similarly, the depth of the crest of a structure will remain uncertain. Figures 16 and 17 show an example of this for the Dhemesticha sub-basin (see figure 1). For the field data based model, 3D constraint on the geometry exists and permits the crest and spill point to be identified more accurately than with 2D data. In contrast, the spacing of the exploration scale 2D seismic data prevents the exact depths from being identified. For this example the result of this geometric uncertainty is a column height of 50% of the true value.

Pore Fluid Pressure

Uncertainty in the column height leads to uncertainty in the pore fluid pressure within a prospect, with implications for trap integrity and well integrity during drilling. For the example of the Dhemesticha sub-basin (figure 16, 18), the difference in predicted column height leads to different estimates in pore fluid pressure due to buoyancy (figure 18). The smaller hydrocarbon column height predicted by the seismically resolvable geometry results in a lower pore fluid pressure than would actually be present (105 psi versus 210 psi), which is important for two reasons. Firstly, the pore fluid pressure within the prospect will be closer to the top seal fracture pressure, and its capillary entry pressure, than anticipated. Depending on how overpressured the reservoir stratigraphy has become during burial, the top seal may have failed, either through mechanical or capillary failure. Secondly, a greater pressure than anticipated would be encountered at a shallower depth during drilling. This may result in the well being underbalanced, allowing an influx of fluids into the well and a pressure 'kick'. For this example however, the differences in pressure between the seismically resolvable geometry and the actual geometry are relatively small, and may well be within standard, planned drilling tolerances (Redmann, 1991).

Tilted Fault Block Reservoir

Many prospects are formed in the tilted footwall blocks of large faults due to the process of footwall uplift. The along-strike decrease in displacement combined with footwall uplift allows 3-way closure against the fault (figure 19). If displacement on the fault is greater than the thickness of the reservoir interval, and the reservoir interval is juxtaposed against an impermeable lithology, then a suitable hydrocarbon trap may exist. In the Gulf of Corinth rift, the footwall block to the Dhoumena fault is an excellent example of along-strike displacement variation, and hence an analogue to a tilted fault block hydrocarbon trap (figure 20). Extrapolation between 2D lines may lead to significant uncertainty in the along-strike displacement geometry, and hence on the validity of interpreted closures.

Using the DEM and fault displacement data it is possible to calculate the theoretical spill points and crest for the Dhoumena fault block, for both the field-based and seismically forward modelled geometries. The spill points are defined as the maximum depth at which the fault block is isolated from adjacent structures (figure 21). The volumetrics, maximum potential column heights (figure 21) and pore fluid pressures (figure 22), can hence be calculated for both geometries. As with the syn-rift reservoir, complexity of the surface representing the top of the reservoir unit leads to a significant disparity in the maximum column height for the two geometries. A greater column than predicted would be present, leading to pore fluid pressure being underestimated (figure 22).

Fault Rock Supported Column Height

For a classic tilted fault block trap the fault provides the fourth direction of closure, typically by juxtaposing the permeable reservoir facies against an impermeable lithology, such as shale, in the hanging wall. The column height which can be supported is controlled by the structural spill point and the top seal integrity. In the situation where the juxtaposed lithology is not impermeable, then the column height which can be supported depends on the sealing capacity of the fault rocks (Yielding et al., 1997; Fisher and Knipe, 1998; Sperrevik et al., 2002; Bretan et al., 2003; Yielding, 2012). This is a function of the fault rock capillary entry pressure and the buoyancy of the hydrocarbon column (Schowalter, 1979; Watts 1987; Fisher et al., 2001; Brown, 2003). Where the buoyancy pressure is greater than the capillary entry pressure ('threshold pressure') hydrocarbon will be imbibed into the fault rock, and can migrate across the fault.

Column height estimation is often conducted by relating threshold pressure, and hence column height, to fault rock clay content, either through direct sample measurements (Sperrevik et al., 2002) or using the Shale Gouge Ratio (SGR) algorithm as a proxy (Bretan et al., 2003). Neither approach is ideal given the inherent heterogeneity of geological systems, with a less deterministic, semi-probabilistic approach being preferred (Childs et al., 2007; Yielding, 2012). Nevertheless, these approaches provide a good mechanism for illustrating the impact of seismic resolution related geometric uncertainty on fault seal prediction.

During reservoir modelling SGR values are determined by stratigraphic properties and fault displacement. Therefore, uncertainty in fault displacement distributions will lead to uncertainty in SGR calculations, and hence in predicted column heights. This is illustrated by comparing the predicted column heights for the Gulf of Corinth outcrop derived geometry and the seismically resolvable geometry. This is again conducted utilising the Dhoumena fault block as an example. Since appropriate data from the field area are not available, a simple synthetic layercake stratigraphy (as may be available during hydrocarbon exploration) composed of interbedded shales and sands (figure 23) is used to populate the outcrop-defined, and seismically resolvable geometries. SGR values are then calculated for the fault plane where the footwall block is juxtaposed against the hanging wall block (figure 24). The along-strike structural spill point (assuming no additional spill points within the footwall, e.g. figure 21) is also shown. A juxtaposition diagram approach (Allan, 1989; Knipe, 1997) is used to generate a fault plane map of the position of juxtaposition seals and potential leak points. The approach of Bretan et al (2003) is used to derive fault threshold pressure from the calculated SGR values, with these values superimposed upon the sand:sand juxtaposition windows (figure 24). A hydrocarbon density of 0.6 g/cm^3 is used to generate the column height that can be supported at every point along the fault, and is hence used in conjunction with the juxtaposition map to estimate the fault rock controlled column height.

The structural spill point for the outcrop-derived fault geometry is controlled by an area of decreased displacement corresponding to the position of a mapped relay zone. Unusually, the fault tip is at a higher elevation than the relay zone (figure 24), hence the relay zone actually increases the depth of the structural spill point in this instance. This leads to the outcrop-derived geometry having a greater column height than the seismically resolvable geometry (540 m versus 490 m), in the situation where the spill point is structurally controlled. However, when the fault rock properties are taken into account, the column height is significantly reduced for both geometries. The fault geometry influences the distribution of the stratigraphy against the fault, resulting in a juxtaposition seal being present at the crest of the structure for the seismically resolvable geometry. This increases the potential column height relative to the outcrop-derived geometry where no crestal juxtaposition seal is present. In this situation, the outcrop-derived geometry can support a smaller hydrocarbon column than the seismically resolvable geometry (110 m versus 190 m).

DISCUSSION

The aims of this study were to use geometries defined through field data collection to demonstrate some of the consequences of fault geometric uncertainty at the scale of hydrocarbon exploration. This has been achieved by using seismic forward modelling to generate a series of synthetic 2D seismic sections across the onshore Gulf of Corinth rift. The uncertainty in the 3D fault geometry when only sparse 2D data is available is evident from the differences in the outcrop-defined, and seismically resolvable models (Figures 11, 12, 14, 15). The uncertainty in fault, and associated syn-rift stratigraphic geometries, leads to uncertainty in volumetric estimates, structural spill points, pore fluid pressure and fault rock supported column heights. In an exploration environment, this would impact both the economic model and any planned appraisal programme.

The specific uncertainties presented herein are applicable to the local Gulf of Corinth geometry, and the petrophysical properties modelled within that geometrical framework. The Corinth rift is itself extremely heterogeneous, with uncertainties identified in one area not necessarily directly applicable to another locality within the rift. Although geometrical uncertainty exists in all situations where only a restricted amount of data is available, the consequences of that uncertainty are not necessarily consistent. For example, the seismically resolvable geometry shown here suggests that the syn-rift facies is relatively isolated between individual sub-basins, contrasting with the 'real' syn-rift geometry which shows high connectivity. However, there is nothing suggesting that syn-rift stratigraphy will always have higher connectivity than can be identified in seismic data, rather that it will depend on the specific geometry in question. Hence, the examples portrayed here are simply an example of the potential implications that may arise from exploration-scale structural uncertainty. These uncertainties are relatively self-evident, with numerous published examples of how they relate to the sparse nature of 2D seismic data (e.g. Needham et al., 1996; Childs et al., 1997; Jolley et al., 2007). A number of studies have utilised 2D seismic forward modelling to generate synthetic seismic across known geometries and facies distributions (Johansen et al., 1994; Hodgetts and Howell, 2000; Alaei and Petersen, 2007) however, few if any use the technique to illustrate the potential uncertainties pertinent to hydrocarbon exploration as described here.

Using the technique of seismic forward modelling to illustrate structural uncertainty is not without its own methodological uncertainties. For example, the observation that faults, formed at the topographic surface (as in Greece) and subsequently buried, would reduce in dip due to compaction of the surrounding stratigraphy. This is not reflected in the model since the outcrop geometries have simply been translated to depth, and hence neither do they say anything about the fault growth history. Although the model from which the synthetic seismic sections have been generated is relatively well constrained by outcrop data, it is still uncertain. This is however, largely irrelevant with respect of the qualitative (rather than quantitative) aims of this manuscript. It is the difference between the synthetic seismic data and the original model used to generate the seismic data that is important.

Other than the generalised uncertainties which have been discussed, a number of additional observations can be made that may be applied more broadly. Displacement profiles are broadly similar for the outcrop-derived and seismically-resolvable fault geometries (Figure 13), although the detail observed at outcrop is significantly greater than can be observed with 2D data. The extrapolation of faults between 2D sections inevitably leads to uncertainty, with structures such as relay zones often being unobserved. The location of fault tips and displacement maxima are also uncertain, resulting in inaccurate estimates of fault displacement: length ratios. In turn, this can impact on the understanding of how a basin evolved (Cowie et al., 2000; Paton and Underhill, 2004). The non-identification of displacement minima tends to lead to the smoothing of fault profiles, and the treatment of fault sets as individual faults, rather than as being composed of multiple segments. This may have the effect of displacement:length ratios being underestimated in 2D seismic data.

Addressing and accounting for the uncertainty in structural geometries is, unlike for petrophysical properties such as porosity and permeability, generally not standard practice within the hydrocarbon industry. A number of approaches are possible for estimating structural uncertainty, such as mechanically modelling fault evolution (Welch et al, 2009) or stochastically incorporating structural features (Manzocchi et al., 2008). However it is the assignment of a range of geologically plausible fault configurations during modelling, and the incorporation of these different geometries within uncertainty workflows, which is critical.

CONCLUSIONS

Synthetic seismic sections across known outcrop geometries highlight the uncertainties when basing a 3D geometric model on 2D data. Extrapolating structural geometries from 2D to 3D is inherently uncertain, with data points often unconsciously viewed as end-members (e.g. maximum/minimum throw values), rather than as discrete values located at an uncertain position within a range of possibilities. Consequently, the range of structural uncertainty is likely to be underestimated when evaluating plays and prospects from 2D data alone. Synthetic sections can provide a useful tool for understanding the potential impact of structural uncertainty in rift settings, with a number of implications highlighted herein;

• Widely spaced 2D sections are unlikely to correspond spatially to features such as displacement minima associated with relay zones. This leads to uncertainty when predicting spill points, structural crests and column heights, as well as identifying the location of sediment entry points into basins.

• The uncertainty in column height, as a result of poorly constrained structural geometry, leads to variations in pore pressure prediction, with implications for drilling strategies.

• The disparities between fault geometries constrained in 3D and those in 2D can lead to significant variation in how stratigraphy is modelled to intersect with, and is mapped onto faults. In turn, fault rock properties, and hence potential supported column heights, may vary considerably.

REFERENCES

AHMED, T., 2010, *Reservoir Engineering Handbook (4th edition)*, Gulf Professional Publishing.

ALAEI, B. and PETERSEN, S. A., 2007, Geological modelling and finite difference forward realization of a regional section from the Zagros fold-and-thrust belt. *Petroleum Geoscience,* **13**, 241-251.

ALLAN, U. S., 1989, Model for hydrocarbon migration and entrapment within faulted structures. *AAPG Bulletin,* **73**, 803-811.

ATHMER, W. and LUTHI, S. M., 2011, The effect of relay ramps on sediment routes and deposition: A review. *Sedimentary Geology,* **242**, 1-17.

BARR, D., 1987, Lithospheric stretching, detached normal faulting and footwall uplift. *Geological Society, London, Special Publications,* **28**, 75-94.

BELL, R. E., MCNEILL, L. C., BULL, J. M., HENSTOCK, T. J., COLLIER, R. E. L. & LEEDER, M. R., 2009, Fault architecture, basin structure and evolution of the Gulf of Corinth Rift, central Greece. *Basin Research,* **21**, 824-855.

BELL, R. E., MCNEILL, L. C., HENSTOCK, T. J. & BULL, J. M., 2011, Comparing extension on multiple time and depth scales in the Corinth Rift, Central Greece. *Geophysical Journal International,* **186**, 463-470.

BREHM, J. A., 2003, The North Brae and Beinn Fields, Block 16/7a, UK North Sea. *Geological Society, London, Memoirs,* **20**, 199-209.

BRETAN, P., YIELDING, G. and JONES, H., 2003, Using calibrated shale gouge ratio to estimate hydrocarbon column heights. *AAPG Bulletin,* **87**, 397-413.

BROWN, A., 2003, Capillary effects on fault-fill sealing. *AAPG Bulletin,* **87**, 381-395.

CARTWRIGHT, J. A., TRUDGILL, B. D. and MANSFIELD, C. S., 1995, Fault growth by segment linkage: an explanation for scatter in maximum displacement and trace length data from the Canyonlands Grabens of SE Utah. *Journal of Structural Geology,* **17**, 1319-1326.

CHILDS, C., WALSH, J. J., MANZOCCHI, T., STRAND, J., NICOL, A., TOMASSO, M., SCHOPFER, M. P. J. and APLIN, A. C., 2007, Definition of a fault permeability predictor from outcrop studies of a faulted turbidite sequence, Taranaki, New Zealand. *Geological Society, London, Special Publications,* **292**, 235-258.

COLLIER, R. E. L. & DART, C. J., 1991, Neogene to Quaternary rifting, sedimentation and uplift in the Corinth Basin,Greece. *Journal of the Geological Society,* **148**, 1049-1065.

COLLIER, R. E. L. & GAWTHORPE, R. L., 1995, Neotectonics, drainage and sedimentation in central Greece: insights into coastal reservoir geometries in syn-rift sequences. *Geological Society, London, Special Publications,* **80**, 165-181.

COWIE, P. A., GUPTA, S. and DAWERS, N. H., 2000, Implications of fault array evolution for synrift depocentre development: insights from a numerical fault growth model. *Basin Research,* **12**, 241-261.

DAWERS, N. H. and UNDERHILL, J. R., 2000, The Role of Fault Interaction and Linkage in Controlling Synrift Stratigraphic Sequences: Late Jurassic, Statfjord East Area, Northern North Sea. *AAPG Bulletin,* **84**, 45-64.

DOMÍNGUEZ, R., 2007, Structural evolution of the Penguins Cluster, UK northern North Sea. *Geological Society, London, Special Publications,* **292**, 25-48.

EHRENBERG, S. N. and NADEAU, P. H., 2005, Sandstone vs. carbonate petroleum reservoirs: A global perspective on porosity-depth and porosity-permeability relationships. *AAPG Bulletin,* **89**, 435-445.

FISHER, Q. J. and KNIPE, R. J., 1998, Fault sealing processes in siliciclastic sediments. *Geological Society, London, Special Publications,* **147**, 117-134.

FISHER, Q. J., HARRIS, S. D., MCALLISTER, E., KNIPE, R. J. and BOLTON, A. J., 2001, Hydrocarbon flow across faults by capillary leakage revisited. *Marine and Petroleum Geology,* **18**, 251-257.

FLETCHER, K. J., 2003, The South Brae Field, Blocks 16/07a, 16/07b, UK North Sea. *Geological Society, London, Memoirs,* **20**, 211-221.

FORD, M., ROHAIS, S., WILLIAMS, E. A., BOURLANGE, S., JOUSSELIN, D., BACKERT, N. & MALARTRE, F., 2012, Tectono-sedimentary evolution of the western Corinth rift (Central Greece). *Basin Research*, **25**, 3-25.

GAWTHORPE, R. L., FRASER, A. J. and COLLIER, R. E. L., 1994, SEQUENCE STRATIGRAPHY IN ACTIVE EXTENSIONAL BASINS - IMPLICATIONS FOR THE INTERPRETATION OF ANCIENT BASIN-FILLS. *Marine and Petroleum Geology,* **11**, 642-658.

GJØYSTDAL, H., DROTTNING, Å., LECOMTE, I. and BRANSTON, M., 2007, Advances in quantitative model-assisted seismic interpretation. *First Break,* **25**, 95-102.

GUPTA, A. and SCHOLZ, C. H., 2000, A model of normal fault interaction based on observations and theory. *Journal of Structural Geology,* **22**, 865-879.

GUPTA, S., UNDERHILL, J.R., SHARP I.R., and GAWTHORPE R.L., 1999, Role of fault interactions in controlling synrift sediment dispersal patterns: Miocene, Abu Alaqa Group, Suez Rift, Sinai, Egypt. *Basin Research,* **11**, 167-189.

HODGETTS, D. and HOWELL, J. A., 2000, Synthetic seismic modelling of a large-scale geological cross-section from the Book Cliffs, Utah, USA. *Petroleum Geoscience,* **6**, 221-229.

INGRAM, G. M. and URAI, J. L., 1999, Top-seal leakage through faults and fractures: the role of mudrock properties. *Geological Society, London, Special Publications,* **158**, 125-135.

JACKSON, J. and MCKENZIE, D., 1983, The geometrical evolution of normal fault systems. *Journal of Structural Geology,* **5**, 471-482.

JACKSON, J. and MCKENZIE, D., 1988, The relationship between plate motions and seismic moment tensors, and the rates of active deformation in the Mediterranean and Middle East. *Geophysical Journal,* **93**, 45-73.

JERVEY, M. T., 1988, QUANTITATIVE GEOLOGICAL MODELING OF SILICICLASTIC ROCK SEQUENCES AND THEIR SEISMIC EXPRESSION. *Sea-Level Changes.* SEPM (Society for Sedimentary Geology).

JOHANSEN, S. E., KIBSGAARD, S., ANDRESEN, A., HENNINGSEN, T. and GRANLI, J. R., 1994, Seismic modeling of a strongly emergent thrust front, West Spitsbergen fold belt, Svalbard. *AAPG Bulletin,* **78**, 1018-1027.

JOLLEY, S. J., DIJK, H., LAMENS, J. H., FISHER, Q. J., MANZOCCHI, T., EIKMANS, H. and HUANG, Y., 2007, Faulting and fault sealing in production simulation models: Brent Province, northern North Sea. *Petroleum Geoscience,* **13**, 321-340.

KNIPE, R. J., 1997, Juxtaposition and seal diagrams to help analyze fault seals in hydrocarbon reservoirs. *AAPG Bulletin,* **81**, 187-195.

KOMINZ, M. A. and PEKAR, S. F., 2001, Oligocene eustasy from two-dimensional sequence stratigraphic backstripping. *Geological Society of America Bulletin,* **113**, 291-304.

KUSZNIR, N. J., MARSDEN, G. and EGAN, S. S., 1991, A flexural-cantilever simple-shear/pure-shear model of continental lithosphere extension: applications to the Jeanne d'Arc Basin, Grand Banks and Viking Graben, North Sea. *Geological Society, London, Special Publications,* **56**, 41-60.

KUSZNIR, N. J., ROBERTS, A. M. and MORLEY, C. K., 1995, Forward and reverse modelling of rift basin formation. *Geological Society, London, Special Publications,* **80**, 33-56.

MANZOCCHI, T., CARTER, J. N., SKORSTAD, A., FJELLVOLL, B., STEPHEN, K. D., HOWELL, J. A., MATTHEWS, J. D., WALSH, J. J., NEPVEU, M., BOS, C., COLE, J., EGBERTS, P., FLINT, S., HERN, C., HOLDEN, L., HOVLAND, H., JACKSON, H., KOLBJORNSEN, O., MACDONALD, A., NELL, P. A. R., ONYEAGORO, K., STRAND, J., SYVERSVEEN, A. R., TCHISTIAKOV, A., YANG, C., YIELDING, G. & ZIMMERMAN, R. W., 2008, Sensitivity of the impact of geological uncertainty on production from faulted and unfaulted shallow-marine oil reservoirs: objectives and methods. *Petroleum Geoscience,* **14**, 3-15.

MCKENZIE, D., 1978, Some remarks on the development of sedimentary basins. *Earth and Planetary Science Letters,* **40**, 25-32.

MCLEOD, A. E., DAWERS, N. H. and UNDERHILL, J. R., 2001, The propagation and linkage of normal faults: insights from the Strathspey-Brent-Statfjord fault array, northern North Sea. *Basin Research,* **12**, 263-284.

MCNEILL, L. C., COLLIER, R. E. L., MARTINI, P. M. D., PANTOSTI, D. & D'ADDEZIO, G., 2005, Recent history of the Eastern Eliki Fault, Gulf of Corinth: geomorphology, palaeoseismology and impact on palaeoenvironments. *Geophysical Journal International,* **161**, 154-166.

MCNEILL, L. C., COTTERILL, C. J., BULL, J. M., HENSTOCK, T. J., BELL, R. & STEFATOS, A., 2007, Geometry and slip rate of the Aigion fault, a young normal fault system in the western Gulf of Corinth. *Geology,* **35**, 355-358.

MIN, B., SHU, L., YIN, H., XIN, W. and ZHANG, D., 2007, Conglomeratic reservoir characterization in the Caiyu field of the Langgu sag, North China. *Marine and Petroleum Geology,* **24**, 579-590.

MORTIMER, E., PATON, DA., SCHOLZ, CA., STRECKER, M. and BLISNIUK, P., 2007, Orthogonal to oblique rifting: effect of rift basin orientation in the evolution of the North basin, Malawi Rift, East Africa, *Basin Research*, **19**, (3), 393-407.

NEEDHAM, D. T., YIELDING, G. and FREEMAN, B., 1996, Analysis of fault geometry and displacement patterns. *Geological Society, London, Special Publications,* **99**, 189-199.

PATON, D.A. and UNDERHILL, J.R., 2004, Role of crustal anisotropy in modifying the structural and sedimentological evolution of extensional basins: the Gamtoos Basin, South Africa, *Basin Research*, **16**, (3), 339-359.

PATON, D.A., 2006, Influence of crustal heterogeneity on normal fault dimensions and evolution: southern South Africa extensional system, *Journal of Structural Geology*, **28**, (5), 868-886.

PEACOCK, D. C. P. and SANDERSON, D. J., 1991, Displacements, segment linkage and relay ramps in normal fault zones. *Journal of Structural Geology,* **13**, 721-733.

REDMANN JR, K. P., 1991, Understanding Kick Tolerance and its Significance in Drilling Planning and Execution. *SPE Drilling Engineering,* **6**, 5.

REUSS, A., 1929, Berechnung der Fließgrenze von Mischkristallen auf Grund der Plastizitätsbedingung für Einkristalle. *ZAMM - Journal of Applied Mathematics and Mechanics / Zeitschrift für Angewandte Mathematik und Mechanik,* **9**, 49-58.

ROBERTS, G. P., 1996, Variation in fault-slip directions along active and segmented normal fault systems. *Journal of Structural Geology,* **18**, 835-845.

SCHOWALTER, T., 1979, Mechanics of Secondary Hydrocarbon Migration and Entrapment. *AAPG Bulletin,* **63**, 723-760.

SHAW, D. B. and WEAVER, C. E., 1965, The mineralogical composition of shales. *Journal of Sedimentary Research,* **35**, 213-222.

SPERREVIK, S., GILLESPIE, P. A., FISHER, Q. J., HALVORSEN, T. and KNIPE, R. J., 2002, Empirical estimation of fault rock properties. *In:* KOESTLER, A. G. and HUNSDALE, R. (eds.) *Hydrocarbon Seal Quantification.*

STRUIJK, A. P. and GREEN, R. T., 1991, The Brent Field, Block 211/29, UK North Sea. *Geological Society, London, Memoirs,* **14**, 63-72.

SWARBRICK, R. E., LAHANN, R. W., O'CONNOR, S. A. and MALLON, A. J., 2010, Role of the Chalk in development of deep overpressure in the Central North Sea. *Geological Society, London, Petroleum Geology Conference series,* **7**, 493-507.

WALSH, J. J., BAILEY, W. R., CHILDS, C., NICOL, A. and BONSON, C. G., 2003, Formation of segmented normal faults: a 3-D perspective. *Journal of Structural Geology,* **25**, 1251-1262.

WATTS, N. L., 1987, Theoretical aspects of cap-rock and fault seals for single- and two-phase hydrocarbon columns. *Marine and Petroleum Geology,* **4**, 274-307.

WELCH, M. J., DAVIES, R. K., KNIPE, R. J. & TUECKMANTEL, C., 2009, A dynamic model for fault nucleation and propagation in a mechanically layered section. *Tectonophysics,* **474**, 473-492.

WOOD, A.M., 2013, The Influence of Fault Geometric Uncertainty on Hydrocarbon Reservoir and Simulation Models. *Doctoral Thesis*, University of Leeds.

WOOD, A.M., 2015, The Missing Complexity in Seismically Imaged Normal Faults: What are the Implications for Geometry and Production Response? *Geological Society, London, Special Publications,* ***421***.

YIELDING, G. and ROBERTS, A., 1992, Footwall uplift during normal faulting - implications for structural geometries in the North Sea. *Structural and Tectonic Modelling and its Application to Petroleum Geology, Norwegian Petroleum Society (NPF) Special Publication,* **1**, 289-304.

YIELDING, G., FREEMAN, B. and NEEDHAM, D. T., 1997, Quantitative fault seal prediction. *AAPG Bulletin,* **81**, 897-917.

YIELDING, G., BRETAN, P. and FREEMAN, B., 2010, Fault seal calibration: a brief review. *Geological Society, London, Special Publications,* **347**, 243-255.

YIELDING, G., 2012, Using probabilistic shale smear modelling to relate SGR predictions of column height to fault-zone heterogeneity. *Petroleum Geoscience,* **18**, 33-42.

ZHANG, Z. and GHASSEMI, A., 2011, Simulation of hydraulic fracture propagation near a natural fracture using virtual multidimensional internal bonds. *International Journal for Numerical and Analytical Methods in Geomechanics,* **35**, 480-495.

ZOEPPRITZ, K., 1919, Erdbebenwellen VII. VIIb. Über Reflexion und Durchgang seismischer Wellen durch Unstetigkeitsflächen. Nachrichten von der Königlichen Gesellschaft der Wissenschaften zu Göttingen, Mathematisch-physikalische Klasse, 66-84.

Figure 1. Map showing distribution of main depositional units and faults used to construct geocellular grid and subsequent synthetic seismic sections. Inset shows field area location on the Peloponnese peninsula, Greece. DF = Dhemesticha fault, DhF = Dhoumena fault, VF = Valimi fault, MPF = Mamoussia-Pirgahki fault, EEF = eastern Eliki fault, WEF = western Eliki fault. From Wood, 2013.

Figure 2. Oblique view of top pre-rift surface and faults within geocellular grid. V.E. = x3. The grid can subsequently be populated with the petrophysical properties appropriate to the pre-, syn-, and post-rift facies as outlined in table 1.

Figure 3. Published depth trends used to condition population of porosity property within the geocellular grid. After Kominz and Pekar, 2001; Ehrenberg and Nadeau, 2005; Min et al., 2007.

Figure 4. Oblique view of examples of populated geocellular grids used during forward modelling process. (A) Porosity, (B) VShale.

Figure 5. Cross-sections through model illustrating pore fluid pressure distribution. (A) Distribution of pre-, syn-, and post rift intervals. The syn-rift is defined as the reservoir interval. (B) Pore fluid pressure. The colour scale is adjusted to highlight pressure differences within the syn-rift interval due to the fluid density contrasts between oil and water. This is highlighted in the expanded insets.

Figure 6. Examples of property cubes converted into seg-y volumes to allow export to seismic forward modelling software. (A) Distribution of pre-, syn-, and post rift intervals. (B) Porosity, (C) VShale.

Figure 7. Oblique view of sections through geocellular grid populated with a porosity property. These sections correspond to the position at which 2D synthetic sections are generated. Sections have a spacing of 5 km.

Figure 8. Coarse scale background model generated using sequential Gaussian simulation. The model is used to account for wave propagation effects between survey-source, target and receiver. Porosity is shown although cubes for pressure, fluid saturation, shale, sand, calcite, and quartz were also generated.

Figure 9. Oblique view of 2D survey geometries with porosity sections for reference.

Figure 10. Comparison of known pre-, syn- and post-rift geometry (A) and the resulting synthetic seismic section (B).

Figure 11. Synthetic seismic sections through the Gulf of Corinth rift geometry defined from field data (Wood, 2013). (A) The syn-rift distribution, top pre-rift surface and fault geometries defined from field data are superimposed onto the seismic sections. (B) The syn-rift distribution as defined by the interpreted surface and fault geometries. 2D sections have a spacing of 5 km.

Figure 12. Comparison of outcrop-derived top pre-rift surface and faults (A), and top pre-rift surface and faults generated from extrapolation of 2D seismic interpretation (B). Although the broad scale

geometries are similar, the seismically resolvable model (B) is significantly simplified relative to the outcrop-derived one (A). (C) Aerial view of an isochore map highlighting the differences between the outcrop-derived (A) and seismically interpreted (B) top pre-rift surfaces. Positive differences are shown in purple, negative in red.

Figure 13. Comparison of displacement: Length plots for the top of the pre-rift surface for selected faults from (A) Outcrop-defined geometry, and (B) Seismically resolvable geometry. Overall the profiles are relatively similar, although much of the detail observed at outcrop is missing at the scale of seismic resolution.

Figure 14. Isochore maps for syn-rift of the field based (A), and synthetic 2D seismic based (B), Gulf of Corinth rift geomodels. Low syn-rift sediment thicknesses along fault strike are indicative of intrabasinal highs potentially due to the presence of late-forming fault overlaps. More consistent along-strike thicknesses are suggestive of earlier fault linkage (Cowie et al., 2000).

Figure 15. Aerial views of syn-rift distribution for field data based model (A) and model derived from 2D synthetic seismic data (B).

Figure 16. Aerial views showing comparison of estimated potential column heights for the Dhemesticha sub-basin based upon the outcrop-derived fault and syn-rift geometry (A) and that based on the synthetic 2D seismic data (B). The shallower crest and deeper structural spill point of the outcrop derived geometry lead to a significantly larger potential column height than that of the 2D seismic based model.

Figure 17. Oblique views of the modelled syn-rift fill in the Dhemesticha sub-basin shown in figure 16. The figure illustrates the difference in the depth of the structural crest, the spill point and the corresponding difference in predicted maximum column height for the outcrop-derived (A), and seismically resolvable (B) geometries.

Figure 18. Plot of pressure versus depth for the outcrop derived and seismically resolvable prospect geometries shown in figure 15. The difference in predicted column height leads to an underestimate in pore fluid pressure for the seismically resolvable geometry relative to the outcrop derived geometry.

Figure 19. Idealised schematic of a tilted fault block trap. Footwall uplift generates relief in the form of a half-dome which abuts the fault plane. Hydrocarbons can fill this dome down to the spill points, which are located at the fault tips where displacement is zero, and in the footwall where uplift is zero.

Figure 20. The Dhoumena fault block provides an excellent analogue for tilted fault block type traps. The footwall crest describes the typical displacement pattern of footwall uplift, with the maximum in the centre, decreasing to zero at the fault tips (A, B). Inset shows the location and direction of the two viewpoints. Approximate orientations of photographs are indicated, with faults dipping at approximately 50 degrees to the North.

Figure 21. Oblique view of top pre-rift surfaces for the outcrop-derived (A) and seismically-derived (B) geometries. The location of the Dhoumena fault footwall tilted fault block trap is indicated, with the structural spill point highlighted. Above the spill point is green, below is blue. (C) and (D) show close up views of the trap for the outcrop-, and seismically-derived geometries, respectively. The depth of the predicted spill points, crests and resulting maximum column heights are indicated, along with the rock volume of the trap.

Figure 22. Pressure versus depth for seismically resolvable and outcrop-derived tilted fault block trap geometries shown in figure 17, assuming that traps are filled to their spill points, and that no there is no additional overpressure.

Figure 23. High net:gross (0.63) synthetic stratigraphy used to populate outcrop and seismically resolvable models. For the purposes of SGR calculation sand is defined as having 10% clay content whilst shale has 70% clay content (Shaw and Weaver, 1965).

Figure 24. Fault-normal views of the Dhoumena fault plane displaying fault properties for both the outcrop-derived and seismically resolvable fault geometries. Properties shown, from top to bottom are: SGR, Juxtaposition, Threshold pressure and predicted column height.

Table 1. Mineralogical fractions used to populate pre-, syn-, and post-rift sequences. The values for the pre-rift assumes an almost entirely carbonate composition, whilst the syn-rift composition is constrained by values observed in the field. Composition for the post-rift stratigraphy is synthetic, but is nevertheless dominated by shale. Where possible porosity is also constrained using visual estimates from optical thin section analysis.

Table 2. Physical properties used for generation of elastic and reflectivity cubes used in the seismic forward modelling process.

Table 3. Geometries used for 2D survey design (O'Dowd, pers. comm.).

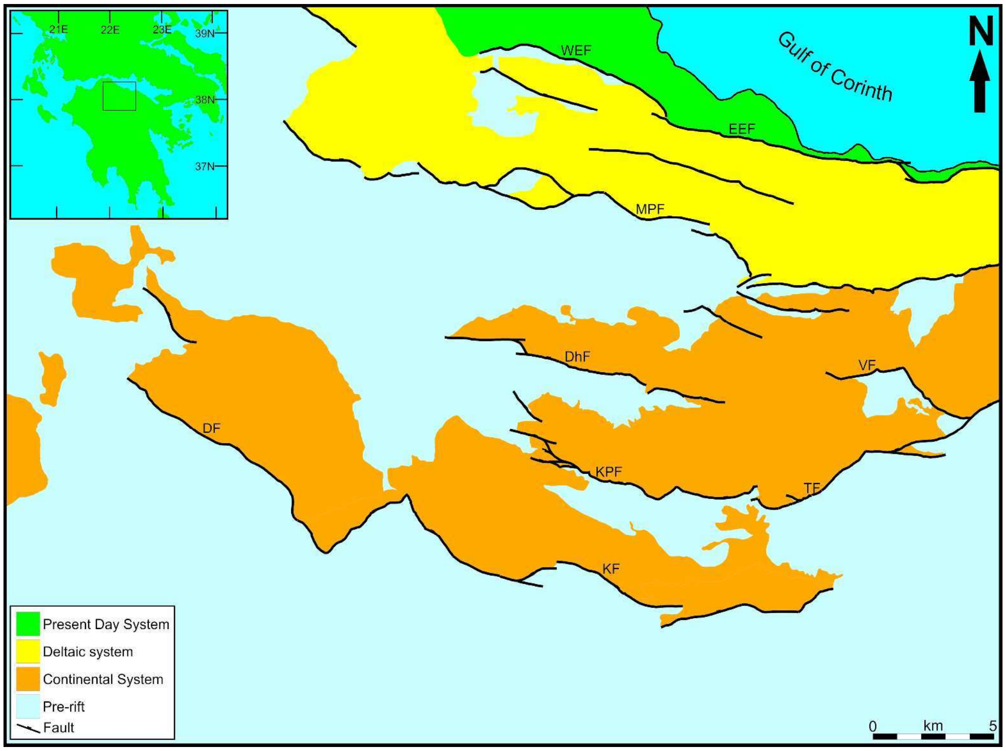

1. Map showing distribution of main depositional units and faults used to construct geocellular grid and subsequent synthetic seismic sections. Inset shows field area location on the Peloponnese peninsula, Greece. DF = Dhemesticha fault, DhF = Dhoumena fault, VF = Valimi fault, MPF = Mamoussia-Pirgahki fault, EEF = eastern Eliki fault, WEF = western Eliki fault. From Wood, 2013.
427x317mm (300 x 300 DPI)

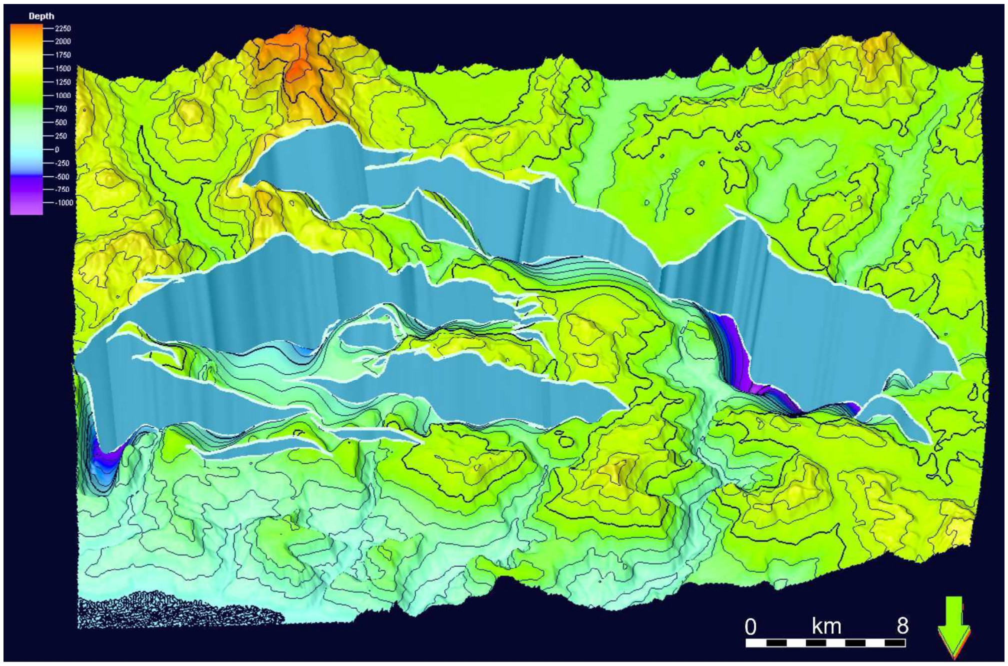

2. Oblique view of top pre-rift surface and faults within geocellular grid. V.E. = x3. The grid can subsequently be populated with the petrophysical properties appropriate to the pre-, syn-, and post-rift facies as outlined in table 1.
372x245mm (300 x 300 DPI)

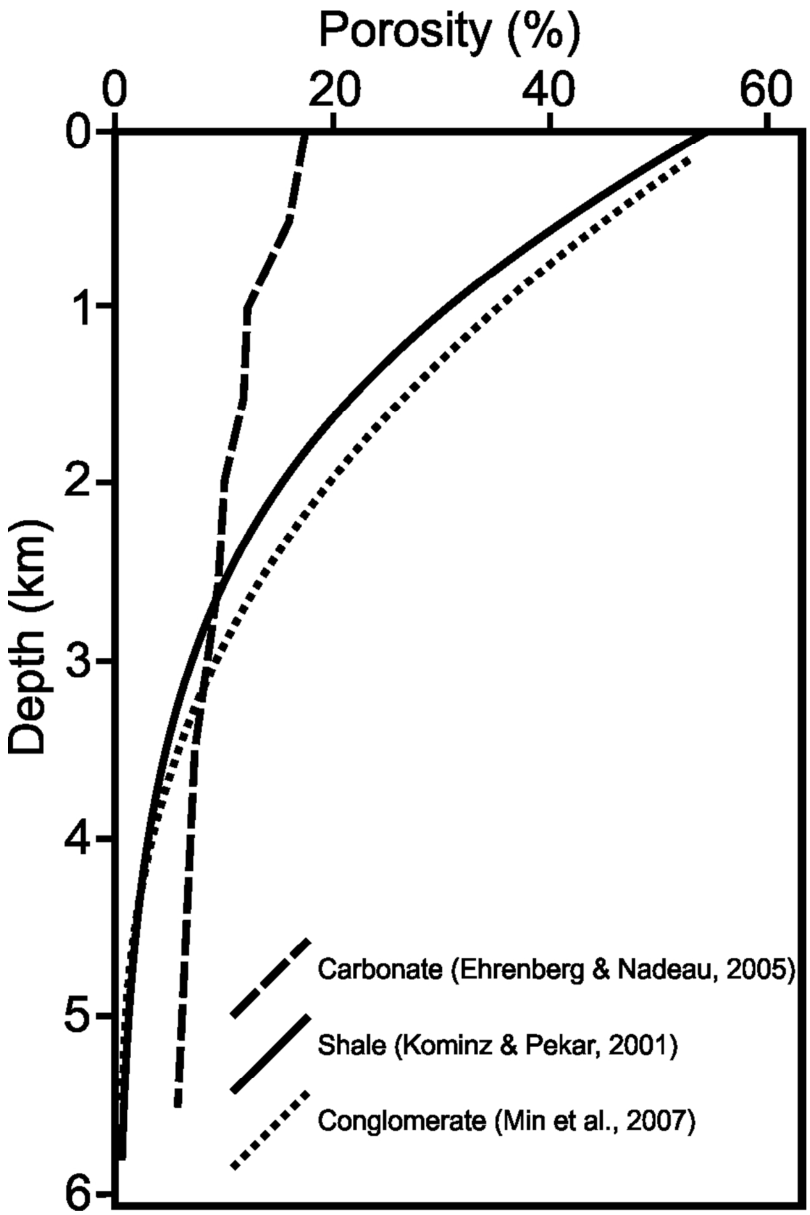

3. Published depth trends used to condition population of porosity property within the geocellular grid. After Kominz and Pekar, 2001; Ehrenberg and Nadeau, 2005; Min et al., 2007.
79x120mm (300 x 300 DPI)

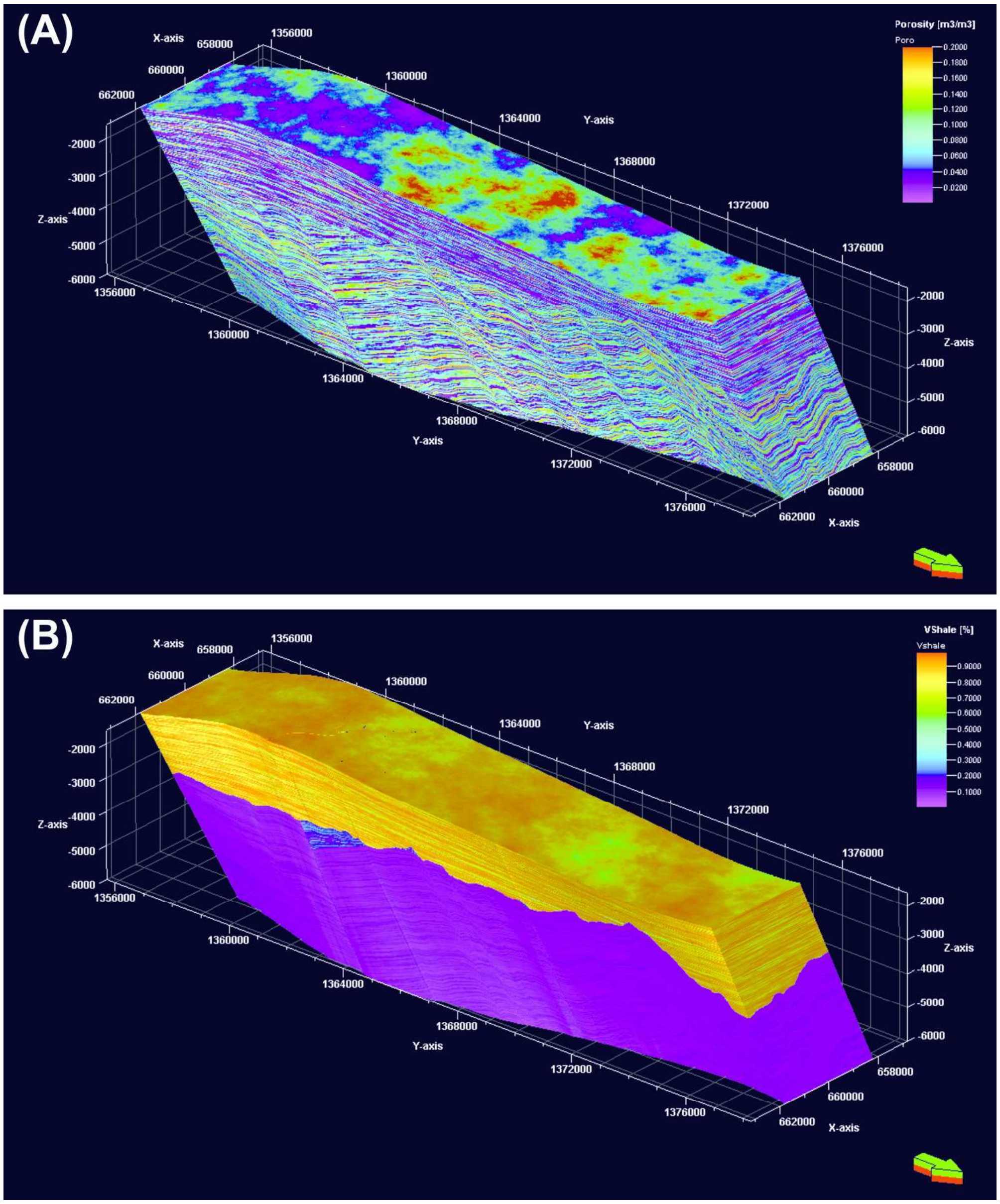

4. Oblique view of examples of populated geocellular grids used during forward modelling process. (A) Porosity, (B) VShale.
170x205mm (300 x 300 DPI)

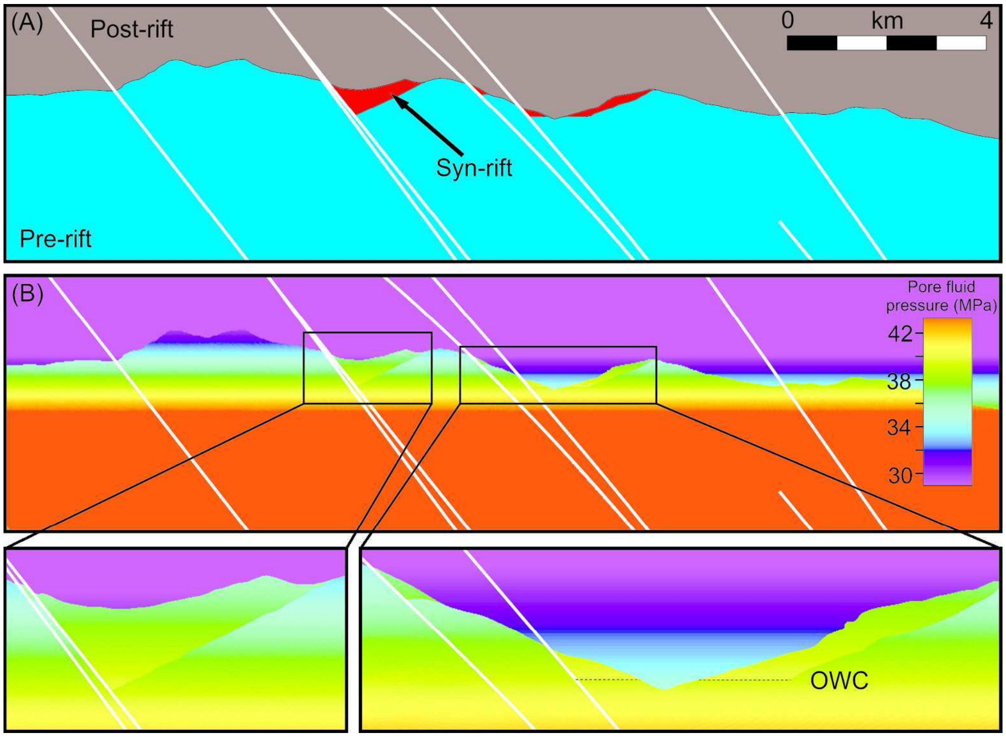

5. Cross-sections through model illustrating pore fluid pressure distribution. (A) Distribution of pre-, syn-, and post rift intervals. The syn-rift is defined as the reservoir interval. (B) Pore fluid pressure. The colour scale is adjusted to highlight pressure differences within the syn-rift interval due to the fluid density contrasts between oil and water. This is highlighted in the expanded insets.
175x128mm (300 x 300 DPI)

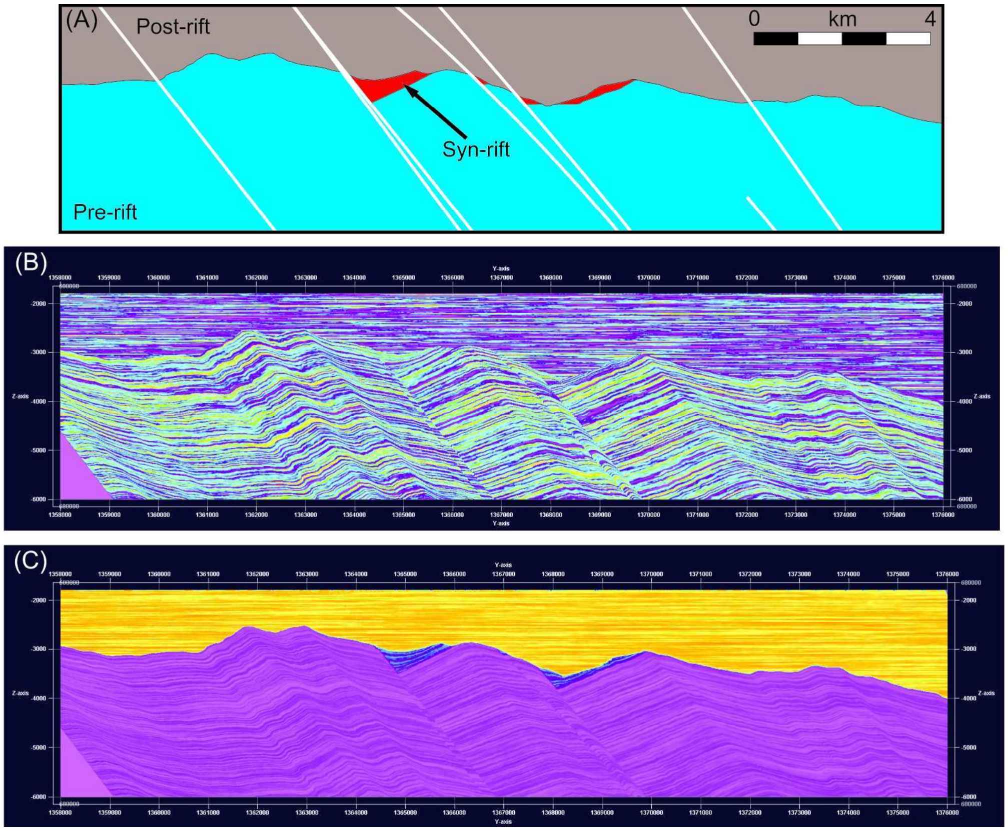

6. Examples of property cubes converted into seg-y volumes to allow export to seismic forward modelling software. (A) Distribution of pre-, syn-, and post rift intervals. (B) Porosity, (C) VShale.
210x173mm (300 x 300 DPI)

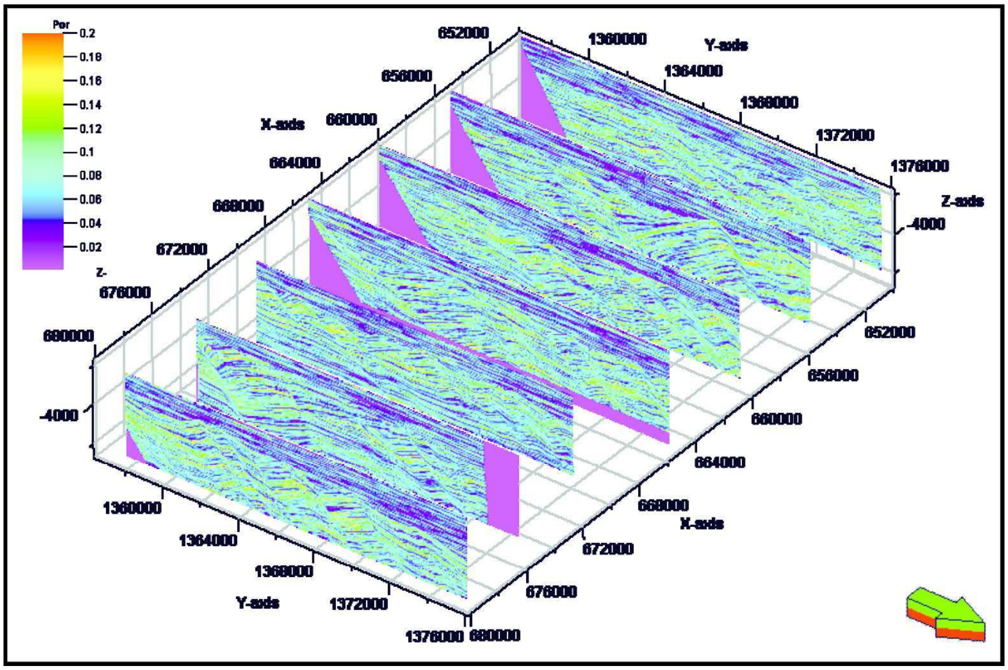

7. Oblique view of sections through geocellular grid populated with a porosity property. These sections correspond to the position at which 2D synthetic sections are generated. Sections have a spacing of 5 km.
219x156mm (300 x 300 DPI)

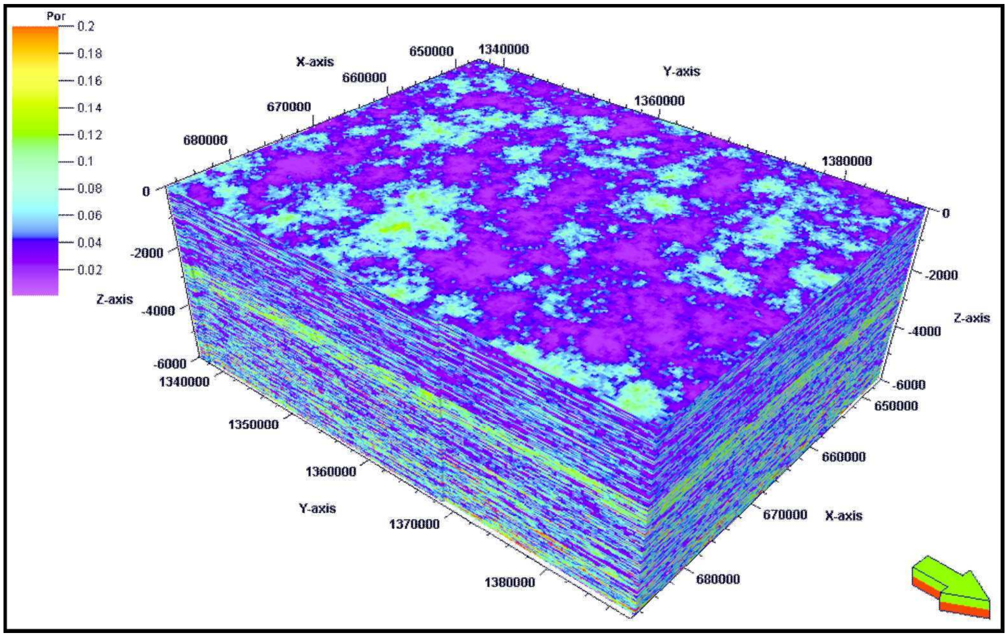

8. Coarse scale background model generated using sequential Gaussian simulation. The model is used to account for wave propagation effects between survey-source, target and receiver. Porosity is shown although cubes for pressure, fluid saturation, shale, sand, calcite, and quartz were also generated.
168x106mm (300 x 300 DPI)

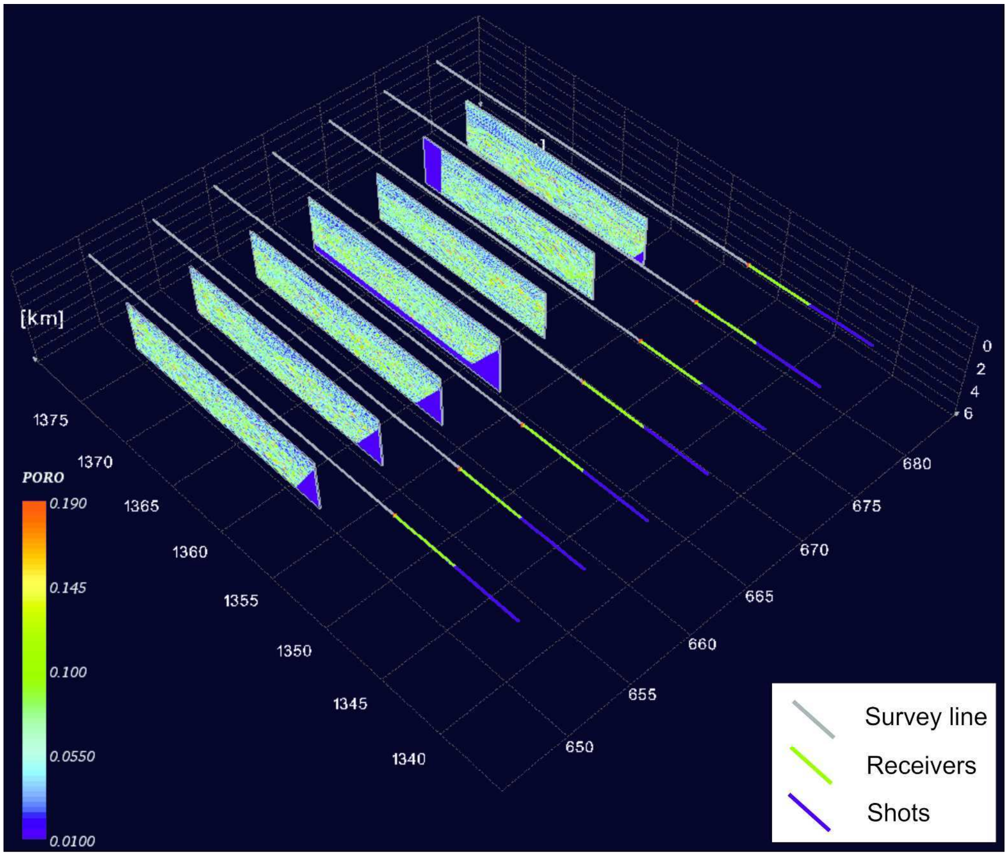

9. Oblique view of 2D survey geometries with porosity sections for reference.
222x188mm (300 x 300 DPI)

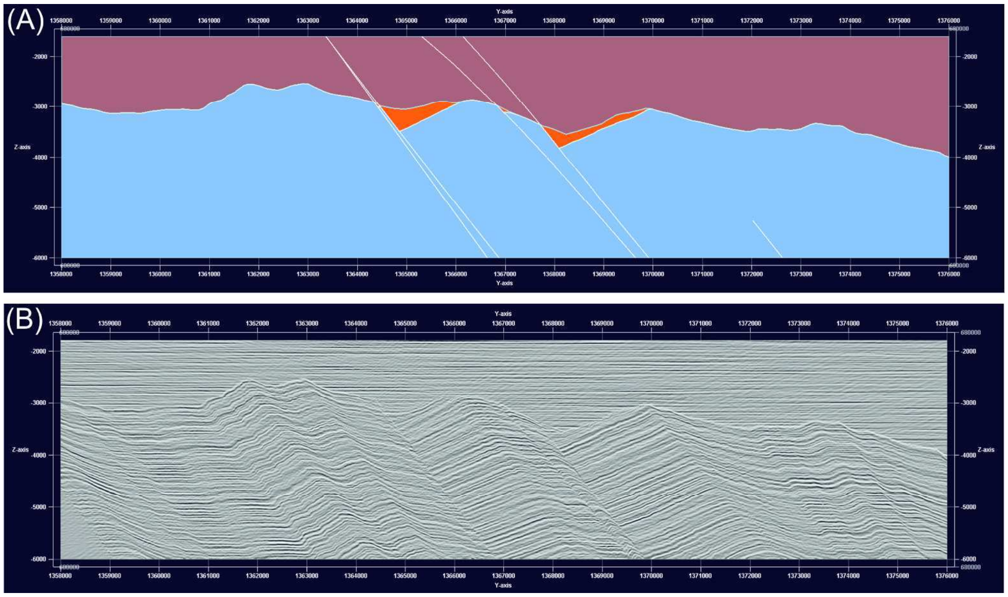

10. Comparison of known pre-, syn- and post-rift geometry (A) and the resulting synthetic seismic section (B).
225x132mm (300 x 300 DPI)

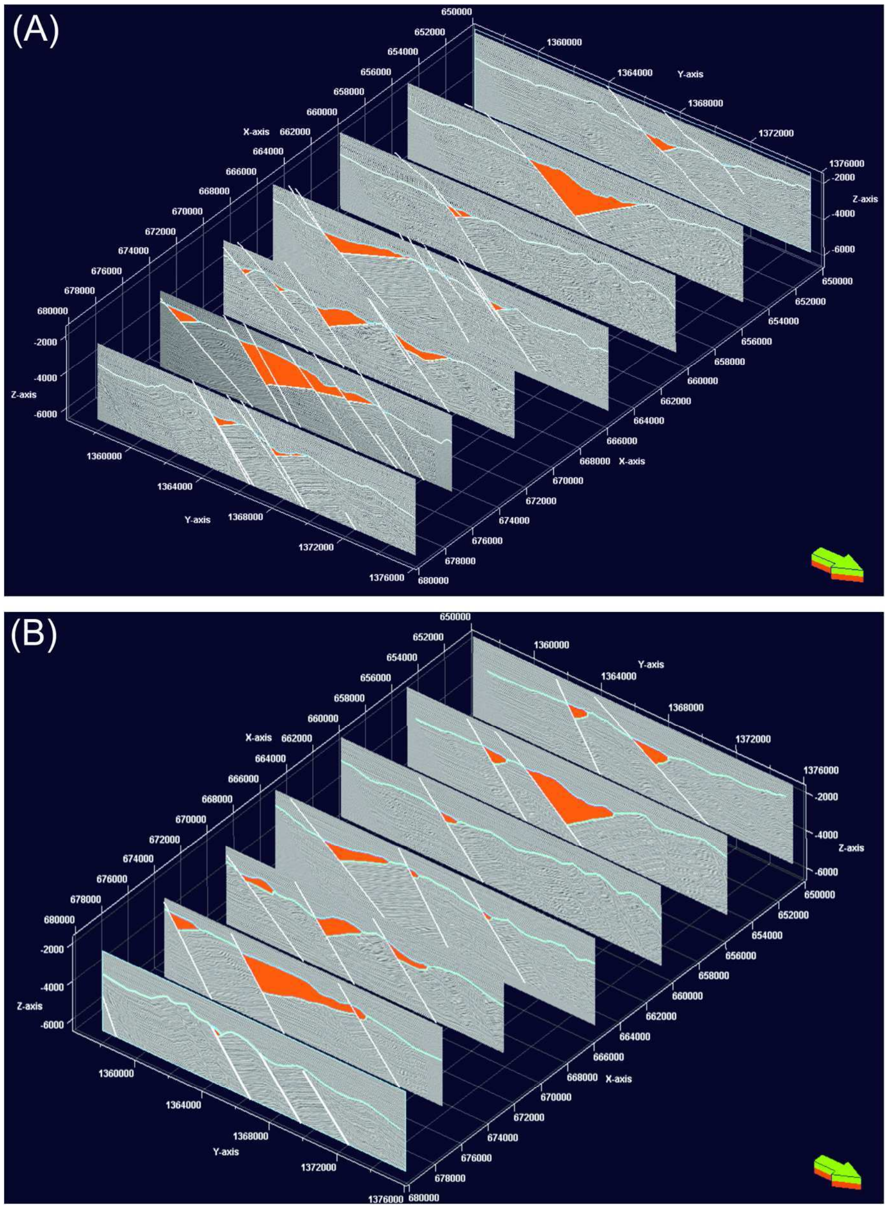

11. Synthetic seismic sections through the Gulf of Corinth rift geometry defined from field data (Wood, 2013). (A) The syn-rift distribution, top pre-rift surface and fault geometries defined from field data are superimposed onto the seismic sections. (B) The syn-rift distribution as defined by the interpreted surface and fault geometries. 2D sections have a spacing of 5 km.
147x200mm (300 x 300 DPI)

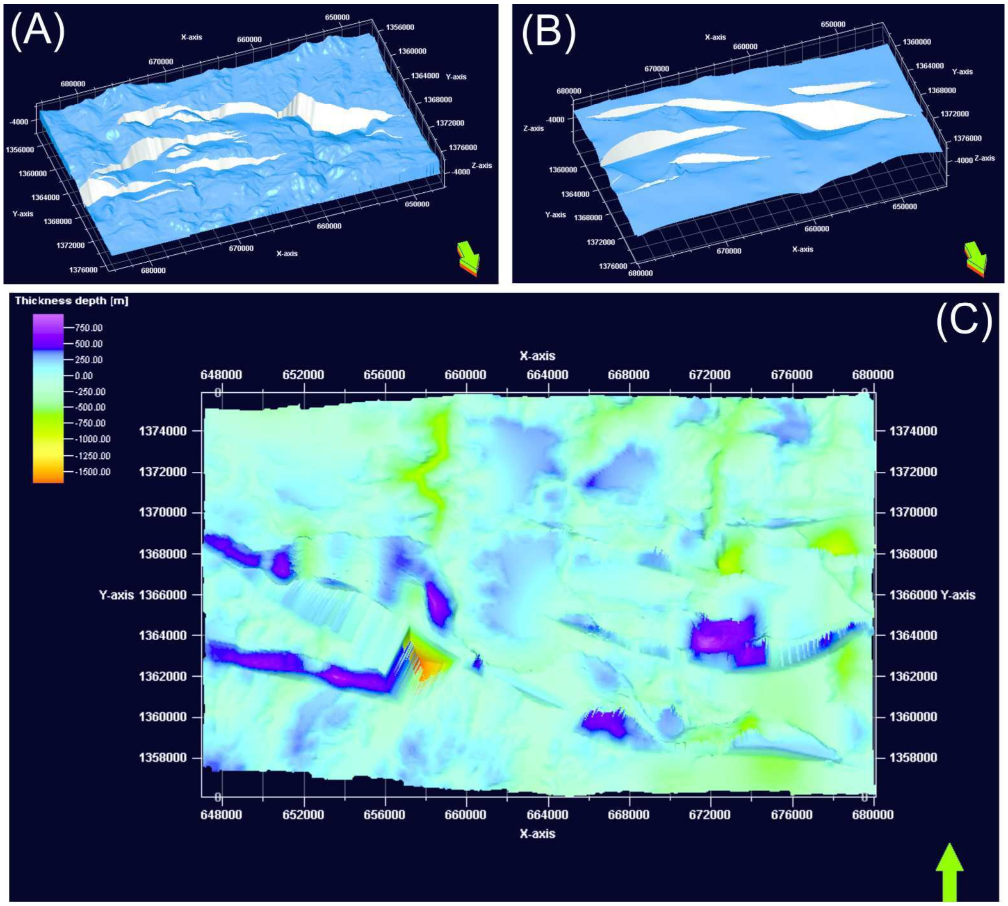

12. Comparison of outcrop-derived top pre-rift surface and faults (A), and top pre-rift surface and faults generated from extrapolation of 2D seismic interpretation (B). Although the broad scale geometries are similar, the seismically resolvable model (B) is significantly simplified relative to the outcrop-derived one (A). (C) Aerial view of an isochore map highlighting the differences between the outcrop-derived (A) and seismically interpreted (B) top pre-rift surfaces. Positive differences are shown in purple, negative in red.
219x197mm (300 x 300 DPI)

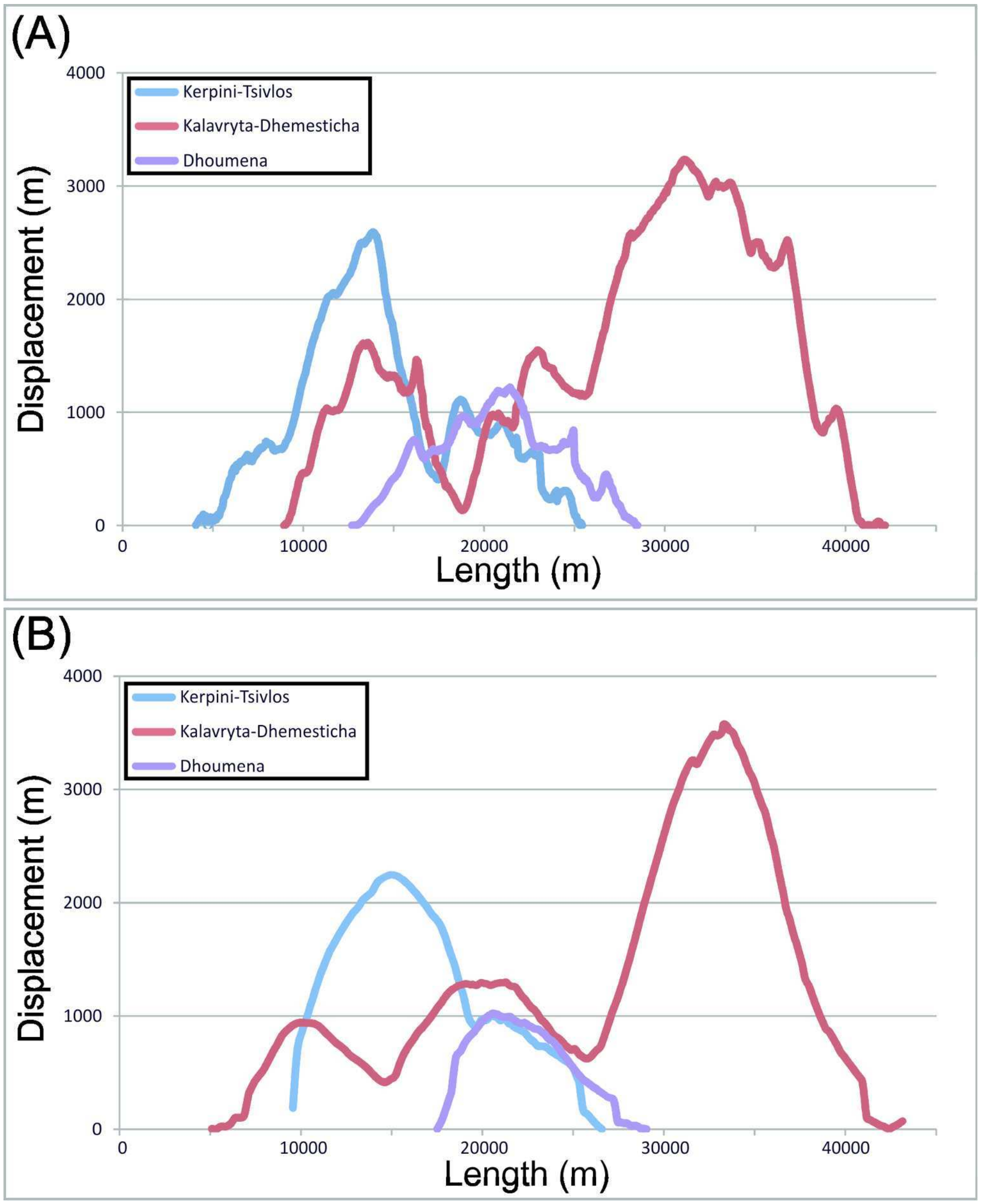

13. Comparison of displacement: Length plots for the top of the pre-rift surface for selected faults from (A) Outcrop-defined geometry, and (B) Seismically resolvable geometry. Overall the profiles are relatively similar, although much of the detail observed at outcrop is missing at the scale of seismic resolution.
163x200mm (300 x 300 DPI)

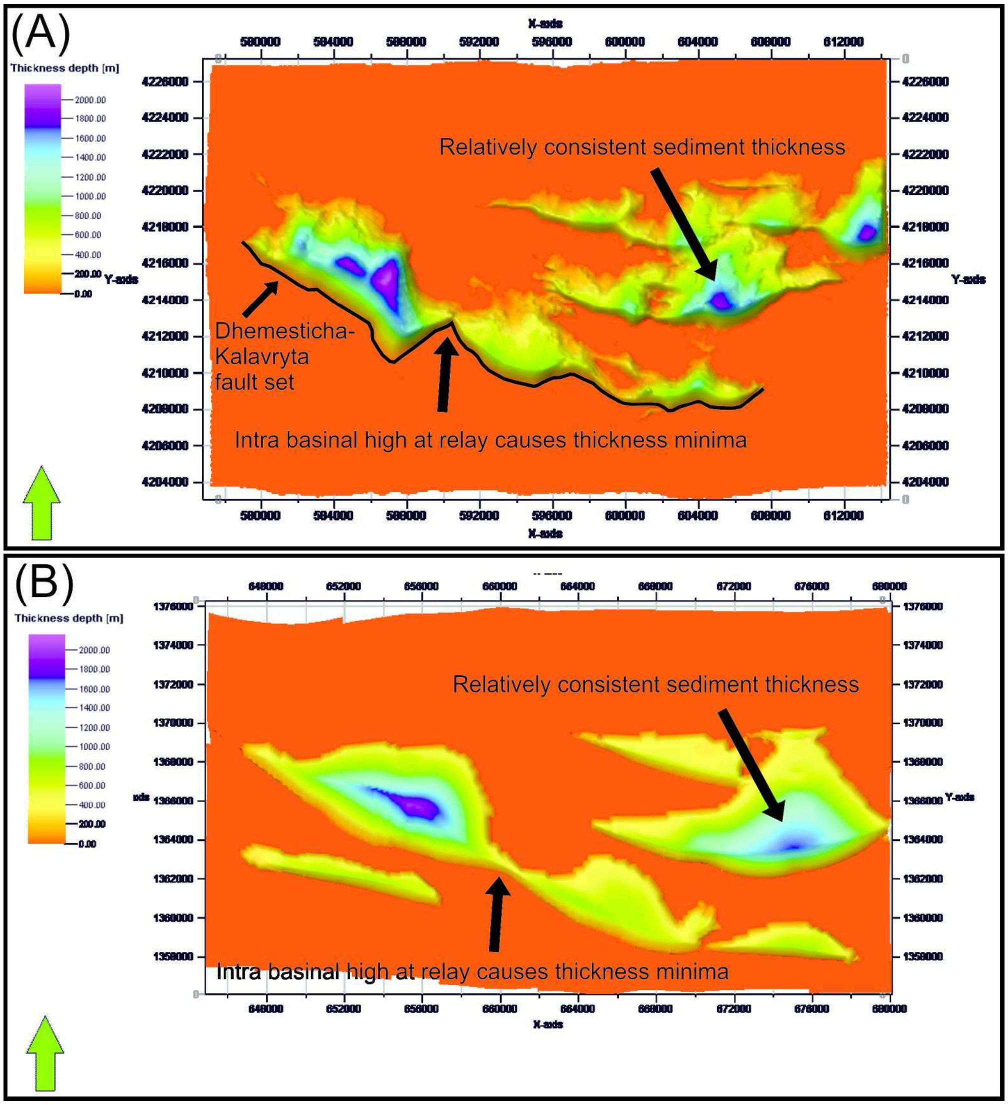

14. Isochore maps for syn-rift of the field based (A), and synthetic 2D seismic based (B), Gulf of Corinth rift geomodels. Low syn-rift sediment thicknesses along fault strike are indicative of intrabasinal highs potentially due to the presence of late-forming fault overlaps. More consistent along-strike thicknesses are suggestive of earlier fault linkage (Cowie et al., 2000).
186x204mm (300 x 300 DPI)

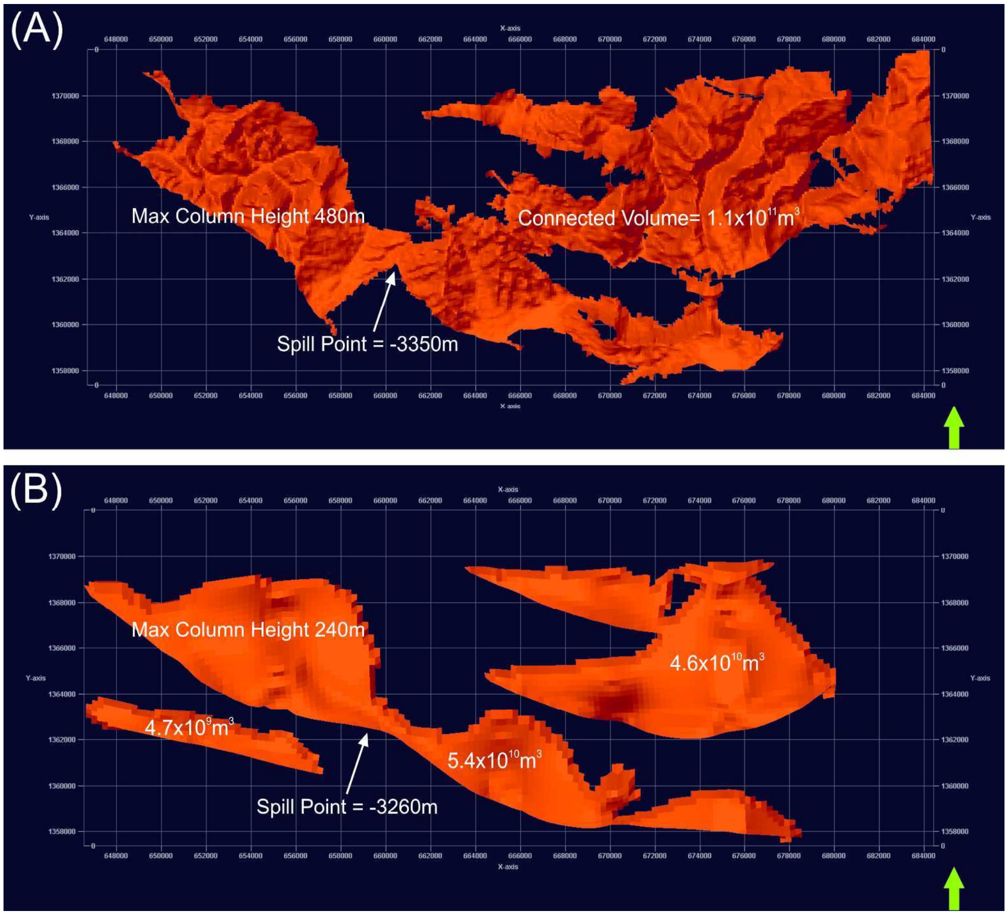

15. Aerial views of syn-rift distribution for field data based model (A) and model derived from 2D synthetic seismic data (B).
235x213mm (300 x 300 DPI)

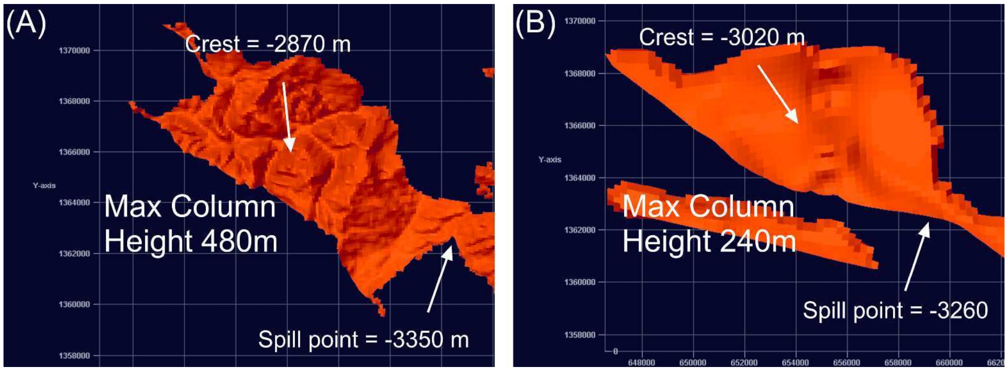

16. Aerial views showing comparison of estimated potential column heights for the Dhemesticha sub-basin based upon the outcrop-derived fault and syn-rift geometry (A) and that based on the synthetic 2D seismic data (B). The shallower crest and deeper structural spill point of the outcrop derived geometry lead to a significantly larger potential column height than that of the 2D seismic based model.
274x99mm (300 x 300 DPI)

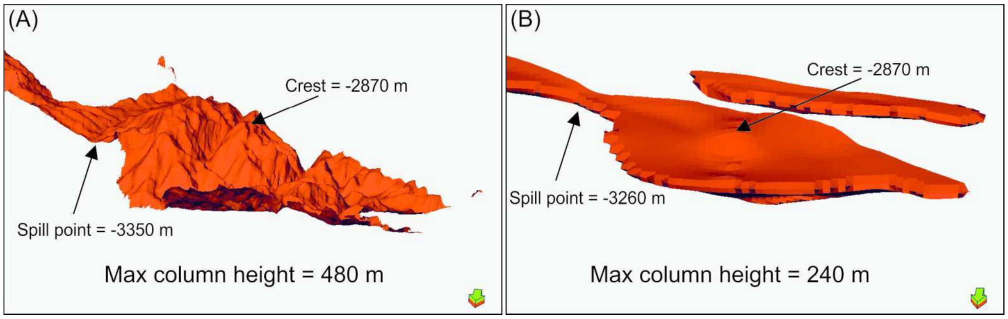

17. Oblique views of the modelled syn-rift fill in the Dhemesticha sub-basin shown in figure 16. The figure illustrates the difference in the depth of the structural crest, the spill point and the corresponding difference in predicted maximum column height for the outcrop-derived (A), and seismically resolvable (B) geometries.
186x57mm (300 x 300 DPI)

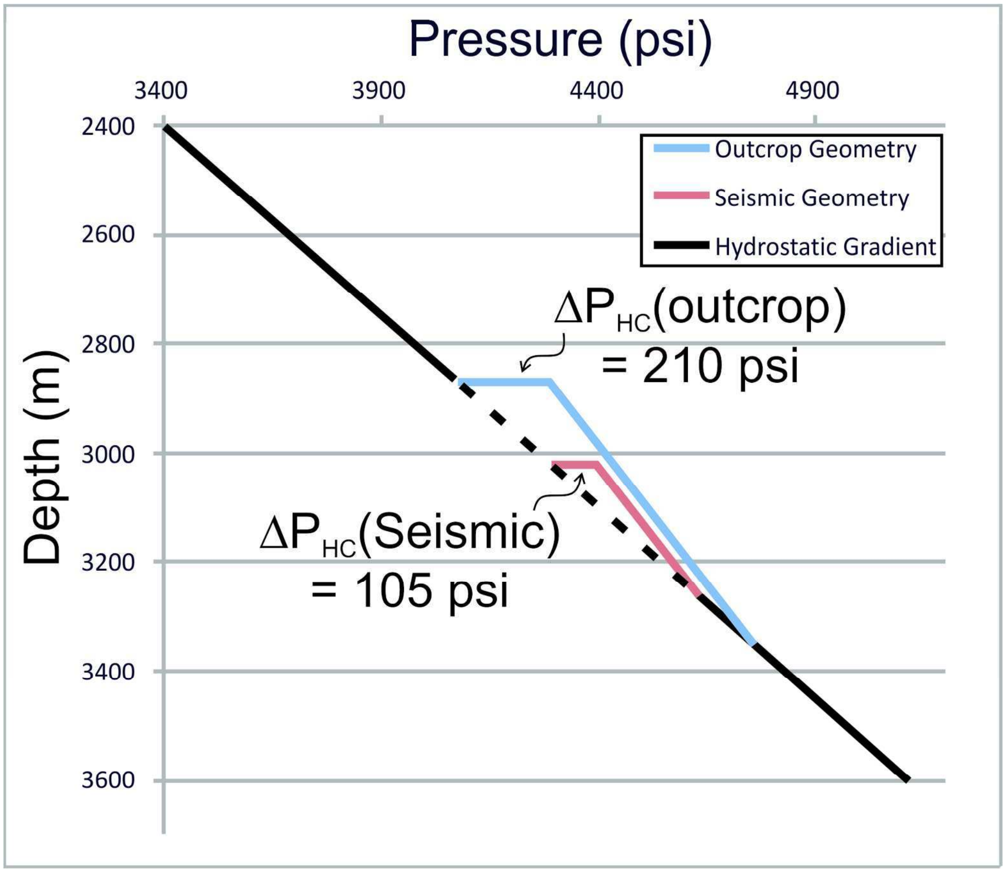

18. Plot of pressure versus depth for the outcrop derived and seismically resolvable prospect geometries shown in figure 15. The difference in predicted column height leads to an underestimate in pore fluid pressure for the seismically resolvable geometry relative to the outcrop derived geometry.
173x149mm (300 x 300 DPI)

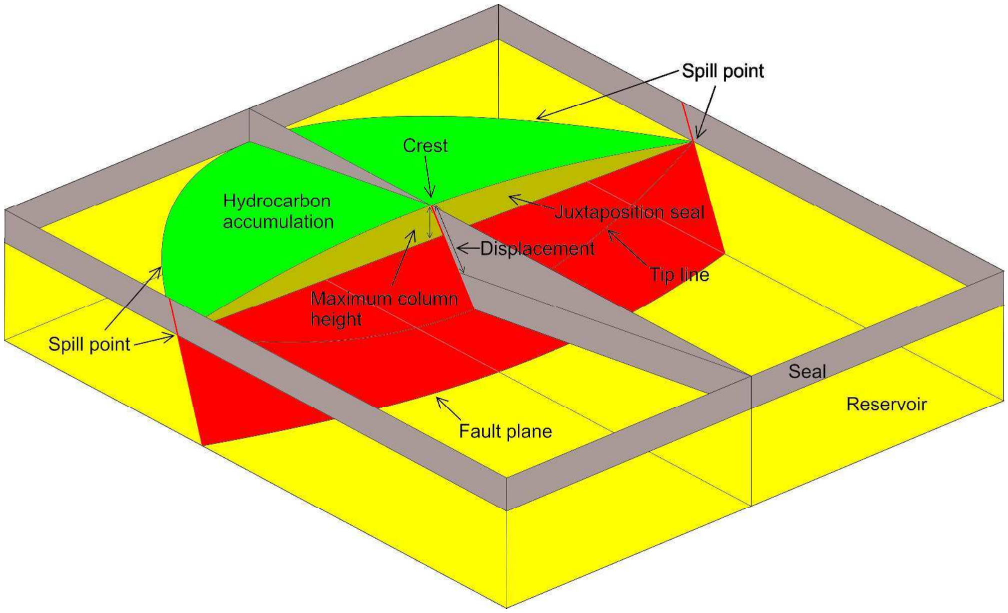

19. Idealised schematic of a tilted fault block trap. Footwall uplift generates relief in the form of a half-dome which abuts the fault plane. Hydrocarbons can fill this dome down to the spill points, which are located at the fault tips where displacement is zero, and in the footwall where uplift is zero.
291x176mm (300 x 300 DPI)

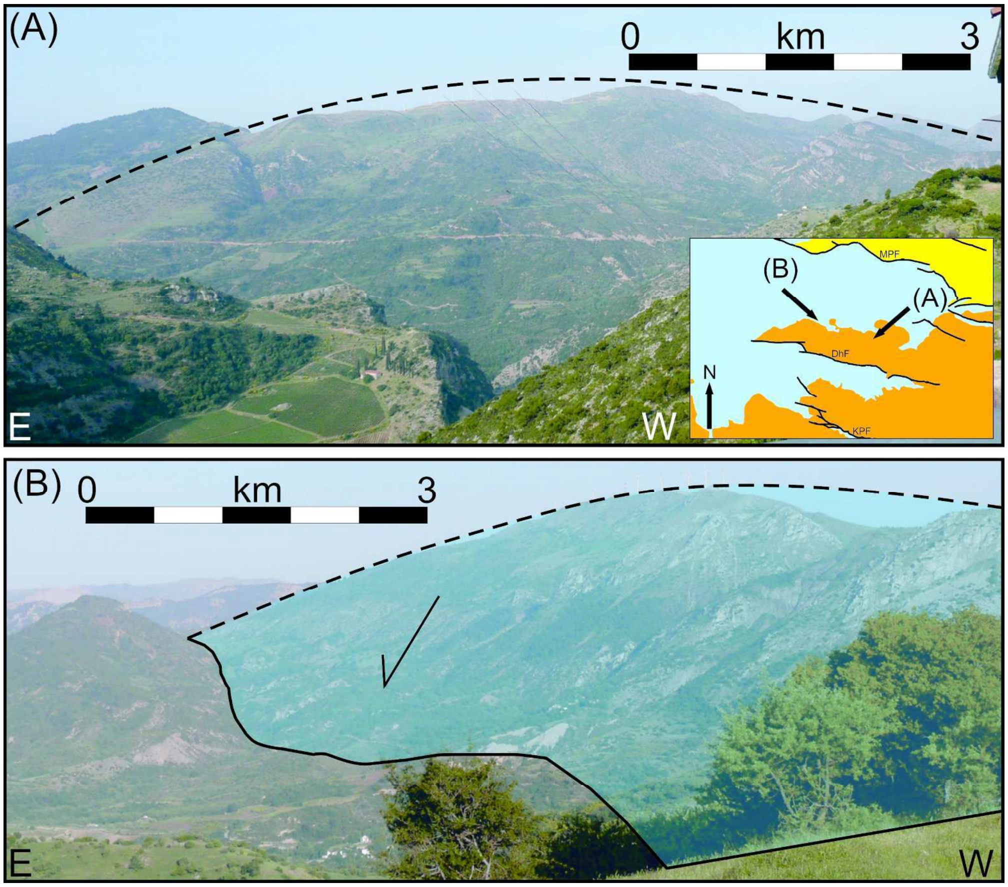

20. The Dhoumena fault block provides an excellent analogue for tilted fault block type traps. The footwall crest describes the typical displacement pattern of footwall uplift, with the maximum in the centre, decreasing to zero at the fault tips (A, B). Inset shows the location and direction of the two viewpoints. Approximate orientations of photographs are indicated, with faults dipping at approximately 50 degrees to the North.
225x198mm (300 x 300 DPI)

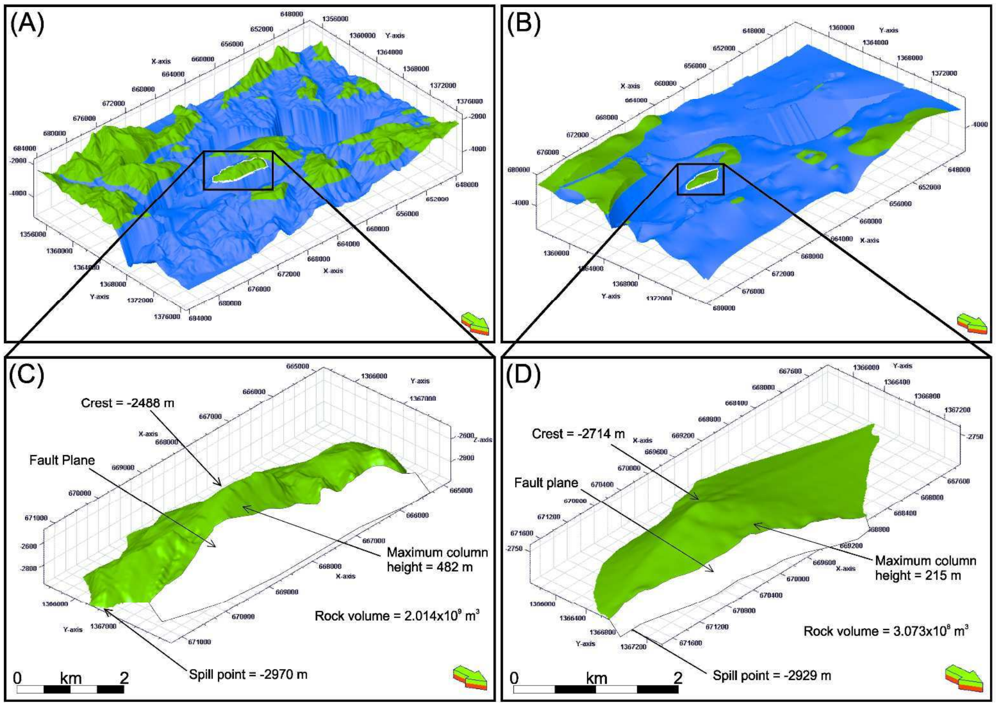

21. Oblique view of top pre-rift surfaces for the outcrop-derived (A) and seismically-derived (B) geometries. The location of the Dhoumena fault footwall tilted fault block trap is indicated, with the structural spill point highlighted. Above the spill point is green, below is blue. (C) and (D) show close up views of the trap for the outcrop-, and seismically-derived geometries, respectively. The depth of the predicted spill points, crests and resulting maximum column heights are indicated, along with the rock volume of the trap.
327x230mm (300 x 300 DPI)

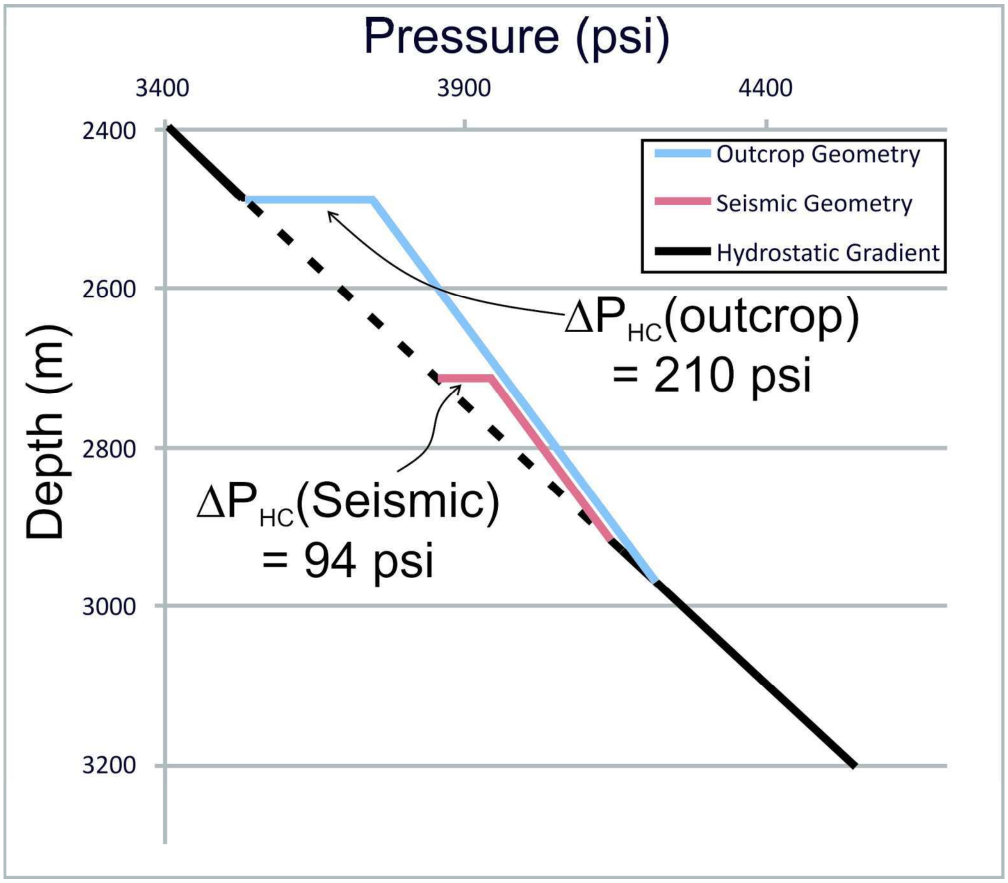

22. Pressure versus depth for seismically resolvable and outcrop-derived tilted fault block trap geometries shown in figure 17, assuming that traps are filled to their spill points, and that no there is no additional overpressure.
171x150mm (300 x 300 DPI)

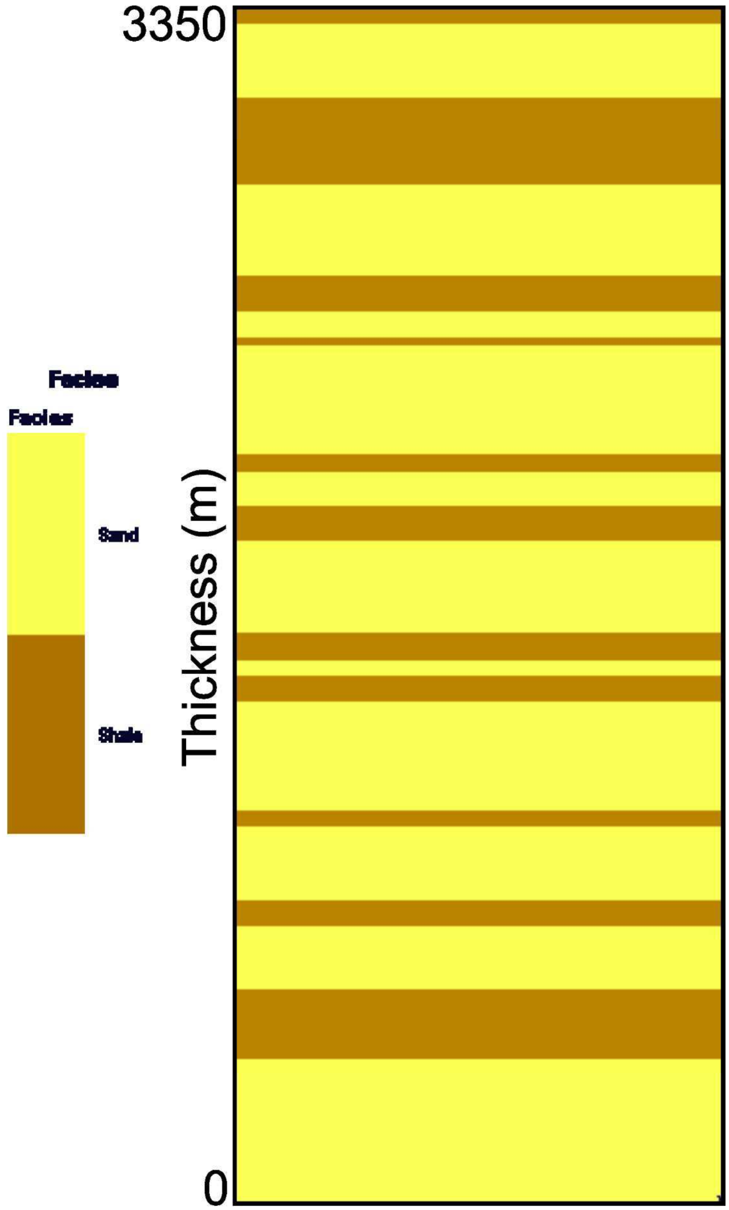

23. High net:gross (0.63) synthetic stratigraphy used to populate outcrop and seismically resolvable models. For the purposes of SGR calculation sand is defined as having 10% clay content whilst shale has 70% clay content (Shaw and Weaver, 1965).
129x213mm (300 x 300 DPI)

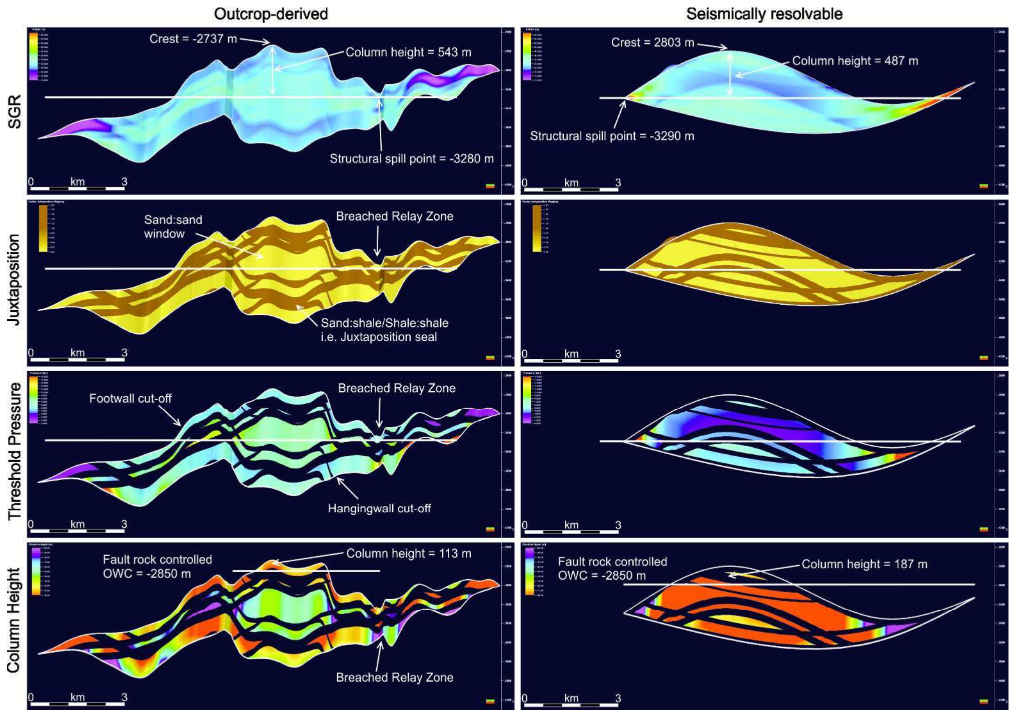

24. Fault-normal views of the Dhoumena fault plane displaying fault properties for both the outcrop-derived and seismically resolvable fault geometries. Properties shown, from top to bottom are: SGR, Juxtaposition, Threshold pressure and predicted column height.
240x168mm (300 x 300 DPI)

	Calcite fraction	Quartz fraction	Sand fraction	Shale fraction	Porosity
Post-rift	0-0.17	0-0.02	0-0.34	0.4414-1	0.0013-0.2
Syn-rift	0.3-0.81	0.09-0.35	0.04-0.14	0.0558-0.21	0.0044-0.15
Pre-rift	0.8-1	0-0.02	0-0.14	0-0.04	0.0053-0.18

Table 1
154x46mm (300 x 300 DPI)

PROPERTY	VALUE
Shale density	2.6 g/cm^3
Sand density	2.65 g/cm^3
Calcite density	2.71 g/cm^3
Quartz density	2.65 g/cm^3
Water density	1.02 g/cm^3
Oil density	0.65 g/cm^3

Table 2
154x61mm (300 x 300 DPI)

Property	Value
Depth	100 m
Offset	100 m
Streamer Length	10000 m
Receiver spacing	25 m
Shot line length	30000 m
Shot spacing	50 m
Input wavelet	40 Hz Ricker

Table 3
154x69mm (300 x 300 DPI)